DEVELOPMENT AND VERIFICATION OF THE LITFIRE CODE FOR PREDICTING THE EFFECTS OF LITHIUM SPILLS IN FUSION REACTOR CONTAINMENTS

by

M. S. Tillack and M. S. Kazimi

July 1980

Plasma Fusion Center

and

Department of Nuclear Engineering

Massachusetts Institute of Technology
Cambridge, Massachusetts 02139

Plasma Fusion Center No. PFC/RR-80-11

DEVELOPMENT AND VERIFICATION OF THE LITFIRE CODE FOR PREDICTING THE EFFECTS OF LITHIUM SPILLS IN FUSION REACTOR CONTAINMENTS

ABSTRACT

LITFIRE is a computer code written to simulate the combustion of lithium in fusion reactor containments. The accuracy of LITFIRE in predicting containment responses has been tested against small-scale spills performed at the Hanford Engineering Development Laboratory.

Based in part on these comparisons, modifications to the code were made to improve its accuracy. Both the chemical reaction rate calculations and the heat transfer mechanisms have been affected. More general improvements were made to extend its applicability, particularly with respect to alternate geometries. The code was expanded to allow for (1) determination of the effects of lithium-concrete reactions, and (2) the existence of a physical separation between the spill area and the containment.

It is found that the modified code temperature field predictions are lower than the original code predictions. However, even the current predictions of lithium-air reaction consequences appear to be conservative in comparison with observations from the small-scale experiments.

TABLE OF CONTENTS

List of Figures

List of Tables

I. INTRODUCTION

The first generation of fusion power plants will almost certainly be based on the D-T fuel cycle, given by:

$$^{2}H + ^{3}H \rightarrow ^{4}He + n + 17.6 \text{ MeV}$$

This is a consequence of the extraordinary difficulty in containing and heating a plasma. D-T ignites at values of $n\tau$* two orders of magnitude lower than the next most promising contender, D-D. Coupled with the fact that D-T ignites at a lower temperature than most other fuels, this implies that the technology required to replace D-T will involve considerable time and effort.

Since tritium (^{3}H) does not occur naturally in sufficient quantities, it must be obtained either externally (such as from fission reactor effuents) or internally through breeding. Table 1.1 lists some tritium producing reactions. Only the lithium reaction offers a real hope of attaining total tritium regeneration.[1] The neutron economy is quite strict, ruling out reactions of low neutron absorption cross section or low utilization fraction. In fact, even with lithium it may be necessary to use neutron multiplication in the blanket via (n,2n) reactions in medium-sized nuclei.

---

* $n\tau$, the Lawson parameter, characterizes the degree of confinement necessary for energy breakeven. For D-T, it is about 6×10^{14} sec/cm^{3} for ignition.

Fortunately, lithium is abundant in salt deposits and in sea water. Metallic lithium also has excellent heat transfer properties which make it a likely candidate for primary coolant as well as breeding medium. (see table 1.2) Combining these two functions will have the added advantage of simplifying the engineering design of the reactor - an important consideration since fusion reactors appear to be far too complex already. Early conceptual designs, such as UWMAK-I and UWMAK-III, took advantage of these properties of lithium by using it as their primary coolant.

Unfortunately, pure lithium is a caustic and highly flammable substance. As is evident from table 1.3, many of the materials and gases likely to be present in controlled thermonuclear reactor (CTR) containments react exothermically with lithium. For the UWMAK-III design, lithium reactions in air and concrete account for the largest potential source of energy with approximately 40,000 GJ available in chemical energy.

In addition, the reaction products of lithium (which may become airborne) are themselves very corrosive. These serious faults of pure lithium have led some of the more recent designers to abandon it in favor of compounds and eutectics of lithium - for example NUMAK and STARFIRE. However, the issue has by no means been set to rest. As fusion research evolves closer to engineering feasibility tests, we need to take a closer look at lithium handling and safety as well as the search for potential alternate coolants.

Some of the many replacements for lithium which are currently under study are listed in table 1.4. Except for lithium and Flibe, the functions of coolant and breeder are separated between two different materials. There are advantages and disadvantages to adopting any of these. In general, the price one pays for the increase in safety is a decrease in breeding capability and inferior heat transfer properties. Whether or not these factors are critical depends upon the particular design.

In order for the reactor designer to make an informed decision on such an important part of the system as the primary coolant and breeding medium, he needs to comprehend all of the aspects of the available choices. It is this concern which motivates the development of the LITFIRE model. LITFIRE is an attempt to quantify the potential consequences of a lithium fire more accurately than previous "first guesses" in order to ascertain just how bad it is.

TABLE 1.1

Potential Tritium Breeding Reactions

^{10}B (n,T) ^{8}Be + 0.2 MeV

^{11}B (n,T) ^{9}Be + 9.6 MeV

^{14}N (n,T) ^{12}C - 4.3 MeV

^{14}N (n,T) 3 ^{4}He - 11.5 MeV

^{6}Li (n,T) ^{4}He + 4.8 MeV

^{7}Li (n, n'T) ^{4}He - 2.5 MeV

$^{2}H + n \longrightarrow {}^{3}H$

^{3}He (n,T) p

ternary fissions, e.g. $^{235}U + n \longrightarrow X + Y + T$

TABLE 1.2

Lithium Properties Favoring its Use as a Coolant

low melting point

high boiling point

low vapor pressure

high specific heat

high thermal conductivity

low density

low viscosity

low activation cross section

low pumping power compared with other liquid metals necessary as a breeding material

TABLE 1.3

Lithium Chemical Reactions

	heat of reaction Kcal/mole of product	
In Air		
$4\ Li + O_2 \rightarrow 2\ Li_2O$	-43	
$2\ Li + O_2 \rightarrow Li_2O_2$	-152	
$6\ Li + N_2 \rightarrow 2\ Li_3N$	-48	
$2\ Li + 2\ H_2O \rightarrow 2\ LiOH + H_2$	-49	
In Concrete		
$8\ Li + Fe_3O_4 \rightarrow 3\ Fe + 4\ Li_2O$	-151.3	(magnetite)
$4\ Li + SiO_2 \rightarrow Si + 2\ Li_2O$		(basalt)
$2\ Li + 2\ H_2O \rightarrow 2\ LiOH + H_2$		
$2\ Li + H_2 \rightarrow 2\ LiH$		
$2\ Li + 2\ LiOH \rightarrow 2\ Li_2O + H_2$		
Others		
$2\ Li + 2\ C \rightarrow Li_2C_2$	-55	
$n\ Li + m\ Pb \rightarrow Li_nPb_m$		

TABLE 1.4

Comparison of Alternate Coolants and Breeding Materials

Material	Breeder Coolant or both	Advantages	Disadvantages
pure lithium	B + C	excellent heat transfer good breeding good neutron moderator no long-term activation no neutron damage	reactive in air and water caustic by-products of fire high electrical conductivity
Flibe[1] (34Be F_2: 66 LiF)	B + C	good moderator marginally good breeding low vapor pressure low electrical conductivity low tritium solubility	scarcity of beryllium chemical reactivity uncertain
Li_2O	B	good packing fraction (good breeding) non-reactive in air	water reaction tritium retention radiation induced sintering reacts with impurities in coolant
$Li\ Al\ O_2$ $Li_2\ Si\ O_3$	B	chemical stability	requires neutron multiplier
$Li_7\ Pb_2$	B	good breeding non-reactive with low-temperature air	reactive in water high pumping power if used as coolant
water	C	large data base	reacts with breeding materials low boiling point and poor heat transfer properties
Helium	C		oxygen and other impurities react with metals & breeding materials high pumping power high pressures

II. LITFIRE DESCRIPTION

2.1 Purpose of the Model

LITFIRE is a computer code developed at MIT[2] to predict the consequences of a postulated lithium spill in a fusion reactor containment. Application of the code allows quantification of the two principal dangers arising from a lithium spill:

1) Lithium combustion may cause overpressurization if heat flow out of the containment gas is sufficiently slow. This could lead to leakage of tritium and activated materials or possibly containment rupture.

2) The heat released in the process of combustion may cause mobilization of the first wall which could contain very large quantities of radionuclides (on the order of 650 million curies estimated for the UWMAK-III design[3] after 2 years operation and ignoring half-lives less than 30 min.). Under extreme conditions this might come about through melting or vaporization. However, a much more likely scenario involves rapid oxidation catalyzed by hot, caustic gases, and subsequent volatilization of the oxides.

Both of these dangers are quantified in LITFIRE through the generation of pressure and temperature profiles in an idealized geometry. By accounting for geometric effects and the various heat transfer mechanisms, LITFIRE makes a much more accurate estimate than earlier, conservative calculations based on an adiabatic equilibrium. Still, the code is small and very simplified. This makes it easy and inexpensive to use, but based on the results presented in Chapter 4, the accuracy is limited to 20 - 30%.

2.2 History of LITFIRE

LITFIRE was first written in 1977 as a modification of the code SPOOLFIRE, developed at Argonne National Laboratory.[4] Since SPOOLFIRE was intended to model sodium fires, the major modification to create LITFIRE was inclusion of lithium-nitrogen and lithium-water vapor reactions, and conversion from sodium to lithium properties. In addition, modeling of the combustion zone and aerosol formation was introduced into the code.

The LITFIRE code was then initially applied to tests of the sensitivity of a CTR containment response to various changes in the parameters characterizing an accident scenario. Conclusions were also drawn concerning the likelihood of various containment responses and the viability of different schemes for mitigating the consequences of a spill. However, the code was not strictly verified in terms of the absolute values of the temperatures and pressures which it predicted.

With experimental data now in hand, the current aim of the LITFIRE development program is to compare the code results with small-scale experiments which simulate larger, full-size spills. These comparisons are made with tests performed at Hanford Engineering Development Laboratory; they are described in full detail in chapter 3.

Several specific goals have been informally laid down for this phase of the program:

a) achieve a 20% accuracy in the LITFIRE temperature field prediction, based on

$$\Delta\% = 100 \times \left| \frac{T_{HEDL} - T_{LITFIRE}}{T_{HEDL,\ max} - T_{HEDL,\ 0}} \right|_{max}$$

b) suggest and implement improvements which will increase the accuracy

c) develop a standard for proper application of LITFIRE for future users.

The fulfillment of these goals is described in the following chapters.

2.3 LITFIRE Model Description

LITFIRE traces the movement of energy from the source to the containment components, and eventually out to the ambient - a constant temperature, infinite heat sink. The source term includes both the hot lithium metal and the fire, also called the combustion zone. In tests without ignition, only the first term is present.

The heat flow mentioned above is computed using one-dimensional heat transfer relations and a combustion source term which is highly idealized. Given enough time and money, the heat transfer mechanisms could be made almost arbitrarily accurate using well-defined correlations and attention to specific details. The source term, on the other hand, is extremely complex and currently not

well-understood. For example, the effects of surface layer formation, wicking, bulk product buildup, and multiple species competition are all very difficult to accurately model. Improvements in these areas are sorely needed, since the accuracy of the temperature profiles is limited by the accuracy of the reaction rate.

In order to follow the containment response, LITFIRE solves a set of coupled equations which describes the simultaneous processes of heat and mass transfer. It uses well-known methods of finite differences for the spacial dimensions, and either Simpson's rule or a Runge-Kutta method in the time domain. Properties are computed at each time step from the integral equation:

$$Y(t) = Y(t_o) + \int_{to}^{t} dt' \frac{dY}{dt'} \quad ,$$

where the rates of change $\frac{dY}{dt}$ are given for each node by finite difference solution of the heat transfer relations.

The physical system is simulated by a nodal network in which each node has a heat capacity equal to that of its physical counterpart and a temperature corresponding to a gross averaged temperature in the structure. Heat flows are calculated between nodes using the values of temperature and of the thermal resistance between any two nodes.

The one-cell version of LITFIRE is shown schematically in Figure 2.1. In general, the three heat transfer mechanisms - conduction, convection, and radiation - are allowed between nodes when-

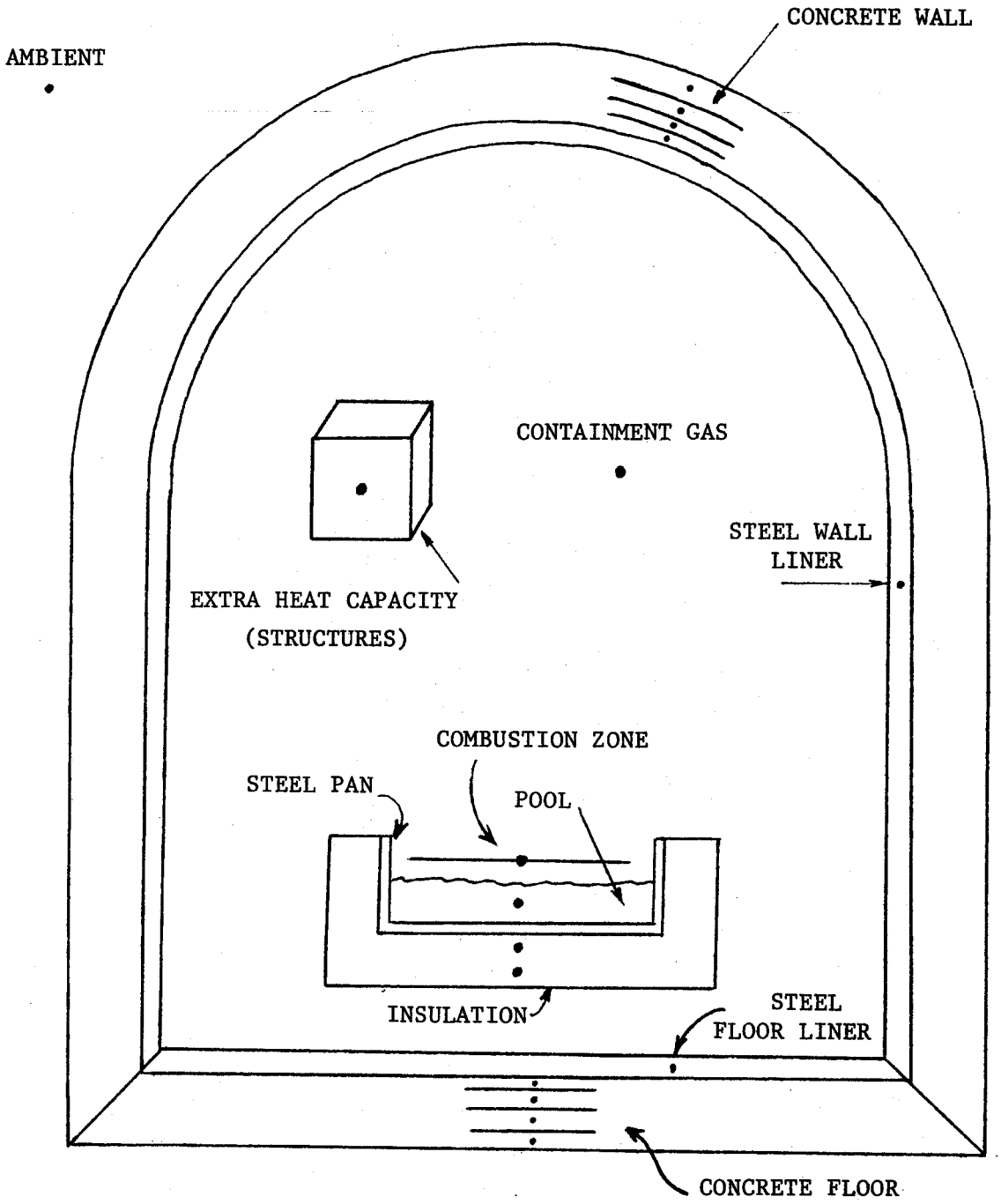

Figure 2.1 One-Cell Node Structure with Suspended pan.

ever appropriate. Exceptions occur when the effect of a particular heat transfer channel is minor. For example, there is no radiation from the extraneous heat capacity node or the outermost concrete node.

2.4 Recent Changes to the LITFIRE Geometry

Most of the nodes appear in the original version of LITFIRE and can be found in reference 2. Some notable exceptions occur in the current version of LITFIRE which make the code more flexible and/or help to model the special features of the HEDL experiment.

1) The number of concrete nodes can now be varied between zero and 20, with each thickness defined by the user. Care must be taken in selecting node sizes such that

$$Fo = \frac{\alpha \Delta t}{(\Delta x)^2} \lesssim 0.3 \qquad \text{where} \qquad \alpha = \frac{\rho c_p}{k}$$

does not violate the minimum step size in the explicit conduction heat transfer calculations (for $\Delta t \sim 0.3$ sec we need $\Delta x \gtrsim 4$ inches).

2) An insulated, suspended spill pan option has been added. If employed there are two insulation nodes of variable thickness and one steel pan node. If not employed, then the lithium is spilled directly onto the floor of the steel liner.

3) An extraneous heat capacity node was added to model structures within the cell volume not

accounted for elsewhere. So far, the effect of this node on the code results has been observed to be negligible.

4) The capability was added to represent discrete injections of gas independent of the containment flooding option for consequences mitigation. These injections were necessary in the HEDL experiment in order that the cell pressure never fell below atmospheric, since it was susceptible to leaking at underpressures. The most pronounced effect of these injections is to decrease the nitrogen reaction rate due to an increased oxygen concentration (O_2 is usually depleted faster than N_2).

5) The lithium pool currently has only one node due to its high thermal conductivity. Tests with a three-node version of the pool showed little variation in temperature through the pool - less than 5°C. The increased restriction on the time step due to thinner pool nodes outweighs the increased accuracy, so the three-node pool has been abandoned.

6) The computations in LITFIRE are in British units. In order to avoid rewriting the code in SI units, we have

added a subroutine which converts input from SI to British and then converts output back to SI before printing.

III. DESCRIPTION OF HEDL EXPERIMENT

3.1 Introduction

Our primary source of data for verifying the LITFIRE code is a series of small-scale lithium spills performed at the Hanford Engineering Development Laboratory (HEDL) Large Sodium Fire Facility (LSFF).[5] Six different tests were performed by introducing ten kilograms of preheated liquid lithium into atmospheres of carbon dioxide, pure nitrogen, and ordinary air. Tables 3.1 and 3.2 summarize the important parameters characterizing each test.

The verification of LITFIRE is based upon measurements taken during each test including temperatures, gas pressure, and spill pan mass. These values were monitored continuously for a 24 hour period following the spills (although combustion was always completed in less than four hours). In addition, discrete measurements were made during and after the tests in order to determine the composition of the reaction pan, aerosol, and bulk gas.

3.2 Description of the HEDL test cell

The diagram of the LSFF (see Figs. 3.1 and 3.2) gives detailed information on the location of the various components of the test cell and associated instrumentation. The most conspicuous element is the steel containment vessel which measures 2.13 m in

TABLE 3.1

HEDL Test Summary

test	LC-1	LN-1	LN-2	LN-3	LA-1	LA-2
species in cell gas	CO_2	N_2	N_2	N_2	normal air	normal air
initial Li temp ^oC	238	222	532	840	243	510
#peak Li temp ^oC	238	224	532	916	1001	977
initial gas temp ^oC	49	38	41	46	27	43
peak gas temp ^oC	48	37	49	82	102	118

or peak pan temp. when thermocouples failed

TABLE 3.2

Classification of Tests

no combustion	single species combustion	multiple species combustion
LC - 1	LN - 3	
LN - 1 *		LA - 1
LN - 2 *		LA - 2

* surface reaction observed

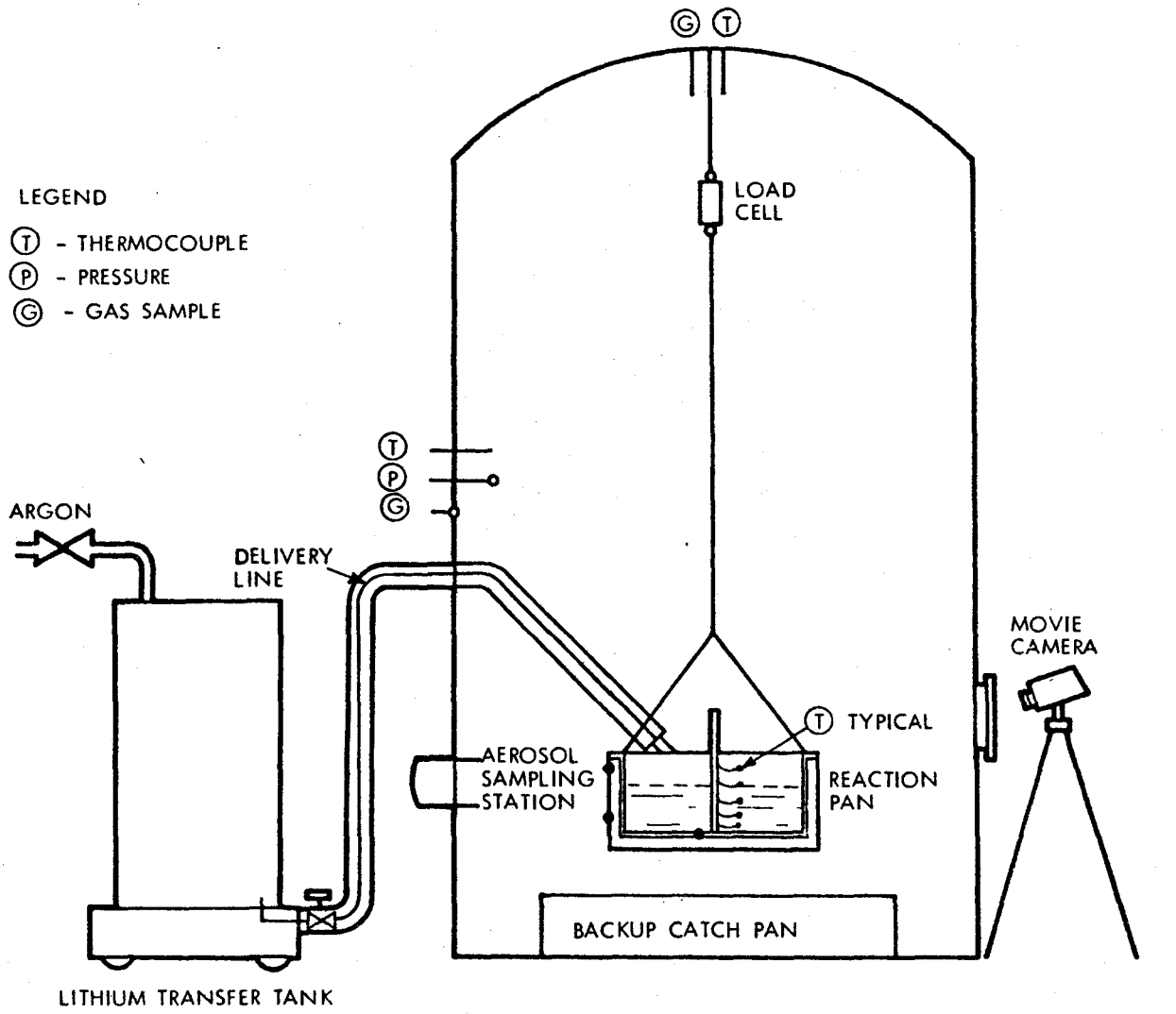

Fig. 3.1 Schematic of Lithium-Atmosphere Reaction Test Equipment Arrangement.

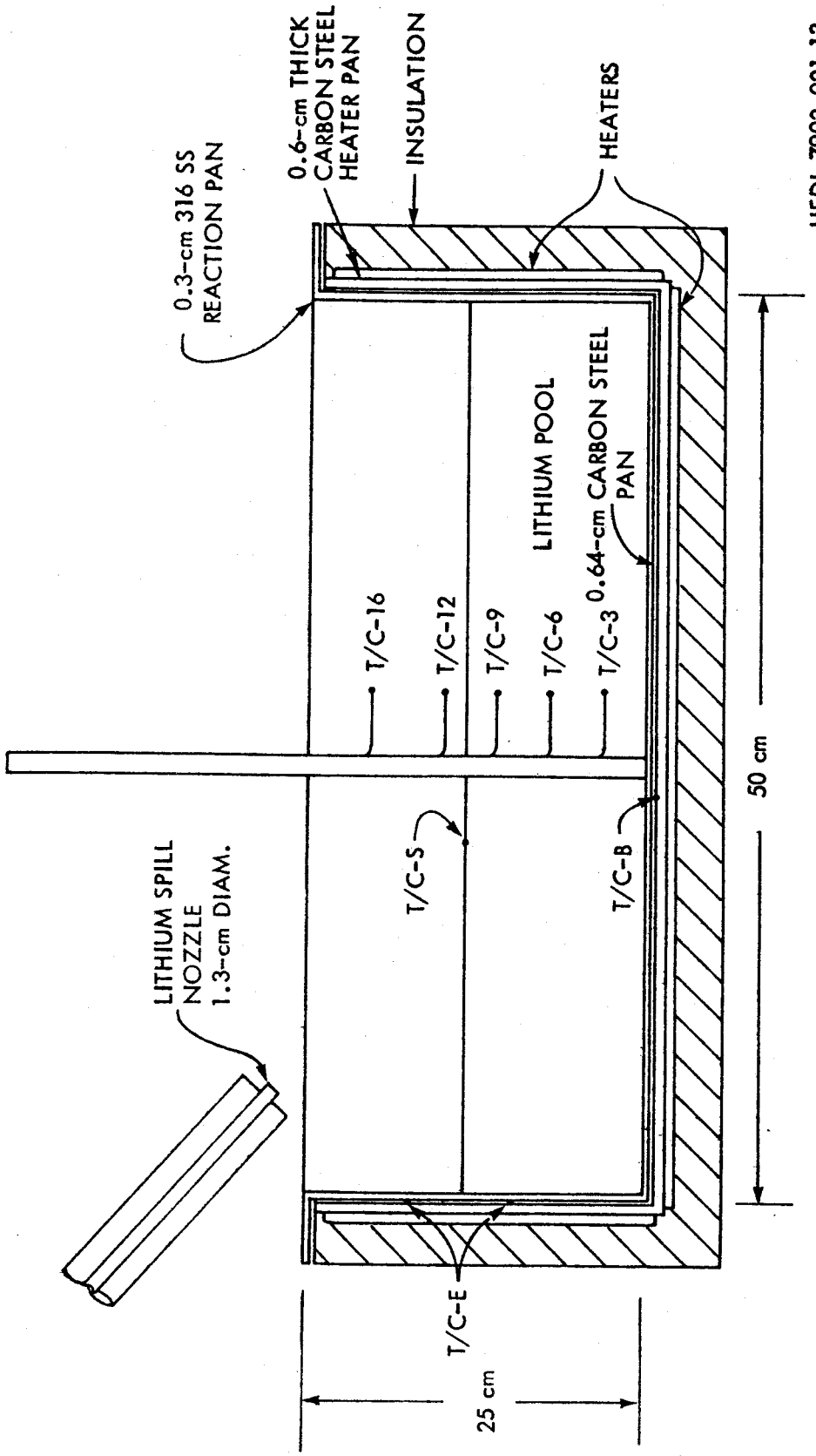

Figure 3.2 Schematic of Lithium-Atmosphere Reaction and Heater Pans.

diameter, 3.7 m high, 8 mm thick, with a volume of 14.1 m^3 - approximately 5.6 x 10^{-5} as big as the UWMAK-III containment. The steel vessel is free to convect and radiate energy directly to the ambient, which in this case is a brick room with a volume of approximately 150 m^3.

Inside the cell hangs a steel spill pan which contains the burning lithium. The spill pan is 50 cm x 40 cm x 25 cm high. It is encased in another tightly fitting steel pan which has heating elements attached to it for preheating the pan. The entire spill pan apparatus is encased on five sides with 7.6 cm of ceramic insulating fiber and suspended by chains to a height of about 60 cm above the floor.

The lithium delivery system consists of a storage tank and a long, insulated 1.8 cm inner diameter delivery tube, both capable of being preheated for each test. The outlet nozzle of the delivery line extends to just above the pan lip. This close proximity to the pool surface, combined with the relatively slow transfer rate ensured that very little spray fire existed. For our comparisons, we assumed no spray fire at all.

3.3 Description of the HEDL Test Procedure

For each of the six tests, the experimental procedure was the same. Before transferring the lithium from the transfer tank

into the spill pan, the cell was filled with the appropriate atmosphere and the lithium, delivery line, and spill pan were all preheated. This preheating was sufficient to guard against unwanted freezing of the lithium. However, as the temperature profiles illustrate, there are still aspects of a transient response present which appear similar to that of a real accident. (Even though we are not comparing directly with reactor-size spills, there are some effects like these which can give us some limited insight.)

After transferring the contents of the holding tank, thermocouples monitored temperatures at various locations in the vessel for the remainder of the test. Five were placed in the center of the pool, supported by a vertical rod. Three were placed in contact with the spill pan, two in the bulk gas - one at 6 ft. and one at 12 ft. - and one thermocouple was placed in contact with the steel vessel 6 ft. up. In addition, a pressure gauge at 5 ft. measured the cell pressure, and the load cell kept track of the total mass of the reaction pan and its contents.

During some of the tests, gases of the same composition as the original charge had to be injected in order to maintain a controlled atmosphere. This is a result of the leakiness of the containment vessel at sub-atmospheric pressures. Any errors due to this procedure have been eliminated by incorporating discrete gas injections

into LITFIRE. Other than these injections, the atmosphere was contained within the cell throughout the entire test.

Post-test analysis of the spill pan and aerosol composition helped to identify which reactions had been present and how much aerosol was formed. In addition, grab samples taken during the tests were analyzed in order to determine the cell gas composition. Unfortunately, these measurements are not sufficiently detailed except to get a rough estimate of the reaction rates as a function of time, temperature, and oxygen concentration. It is quite difficult to unravel the combined effects which drive the reaction rate unless a well-controlled experiment is designed for that specific purpose.

3.4 Modelling of the HEDL Experiment in LITFIRE

The difficulties encountered in modelling the HEDL tests are noteworthy not just because of the sheer amount of work expended to solve them, but because they shed much light on the interpretation of the results of the verification study which follows. There are important limitations on the accuracy of the modelling, with which we should be acquainted. Furthermore, since the ultimate goal of our study involves reactor concepts, we should appreciate the applicability of the results when extrapolated to much different sizes and geometries. In the following, we classify these points into two

sections: (1) changes in the LITFIRE model to accommodate the HEDL experiment, and (2) difficulties which could not be incorporated into the model.

3.4.1 Geometric Considerations

a) scaling

It is obvious from Figure 3.1 that the LSFF does not correspond precisely with the geometry of a fusion reactor containment. The small size alone should forwarn us that some effects relating to the physical dimensions may be either ignored or overemphasized. For example, a reactor-sized containment has a much smaller wall surface area to volume ratio. This has the same effect as insulating the cell, since less heat is conducted out this channel. Another scaling effect which might take place concerns the very important paremeter of gas emissivity. The path length of radiation to the walls from the combustion zone scales as the radius, r, whereas aerosol accumulation scales as $1/r$ ($\frac{\text{production rate}}{\text{volume}} \sim \frac{r^2}{r^3}$). Then at reactor sizes we might expect less heating of the gas due to radiation. As we shall see, radiation heating can be the dominant effect on the cell gas.

b) concrete

Another important geometric consideration is that the LSFF has no concrete surrounding the vessel. In the HEDL experiment, this enhances the rate at which energy reaches the ambient, keeping the

cell cool and underpressurized. It is much less likely in a reactor containment that underpressures will be encountered unless active cooling is performed on the cell gas.

c) suspended pan

The presence of an insulated spill pan removes conduction as an avenue of heat transfer out of the pool. This absence heightens the effects of radiation and convection supporting the scaling effect of the gas emissivity. It also keeps the spill localized and deep. The depth of the pool (10 cm) affects all heat transfer mechanisms since all depend linearly upon surface area. The deeper pan delays the extinguishment of the fire and softens some of the transient effects.

d) Extraneous Structures

Besides the spill pan, there are various elements in the HEDL test cell such as: the load cell, delivery line, backup catch pan, chains, and flanges. Actually this is not much different than a reactor containment, where there are numerous extraneous heat sinks dispersed throughout the room. These structures will tend to hold down the gas temperature and give extra inertia to the response.

The modelling of an extra heat capacity node, as well as the suspended spill pan and no concrete options have all been incorporated into the LITFIRE model as described in Chapter II. Therefore, we don't expect these elements to add any innaccuracy to the comparisons

with the HEDL data. However, it deserves to be reiterated that with the reactor in mind as our ultimate concern, these differences will tend to make our conclusions somewhat less applicable.

3.4.2 Idealization in the LITFIRE Model

There is another class of diffitulties which could not be incorporated into the model; they deal with imprecision and the effects of idealizing a rather complex system into a few simplified nodes. The net effect of all the uncertainties is to limit the accuracy of the code, even if all the modelling assumptions are exactly correct, which they are not.

a) Node Shapes

LITFIRE is essentially one dimensional in that the shapes of the various nodes are ignored. The phenomena most affected by geometry is convection, however radiation from the spill pan is also affected. In order to surmount the difficulty with convection, most nodes are given their own heat transfer correlation coefficient "C" in

$$Nu = C\ (Gr\ Pr)^{1/3}$$

This allows the programmer some flexibility in dealing with irregular surfaces, enclosure effects, and other non-ideal conditions. For example, the HEDL containment vessel rests on cement blocks high enough to allow ventilation, but much too close to the ground to assume normal free convection from a horizontal surface. A first

order correction would be to simply reduce the constant C to some smaller value.

The presence of the spill pan complicates the process of gas convection in the containment. But it also makes the radiation view factors more inexact. For simplicity, we assume that the pan sides and bottom radiate only to the cell floor; the pool radiates only to the cell wall and ceiling. In addition, because the pan is so close to the floor (~ 2 ft.), we assume no absorption in the gas due to the pan sides and bottom. (see Figure 3.3)

b) Node Sizes

The large node sizes in LITFIRE introduce a sizeable error due to temperature variations in that element. This problem is especially large in the reaction pan, cell gas, and insulation nodes. For instance, the HEDL data shows for test LA-2 a 75 °C variation in the pan steel (out of 900 °C) at 2 hours into the test, and about 5 °C (out of 100 °C) variation in the cell gas. Across the insulation LITFIRE predicts temperature drops of over 500 °C. The effect on convection and radiation from the insulation can be substantial unless the outer node is kept quite thin. If future experiments are analyzed with an insulated spill pan, it would be worth the effort to add one or two nodes in the insulation.

c) Localization of Measurement

A related problem to the homogenized nodes is the fact that measurements are localized to a single point. Therefore, the error

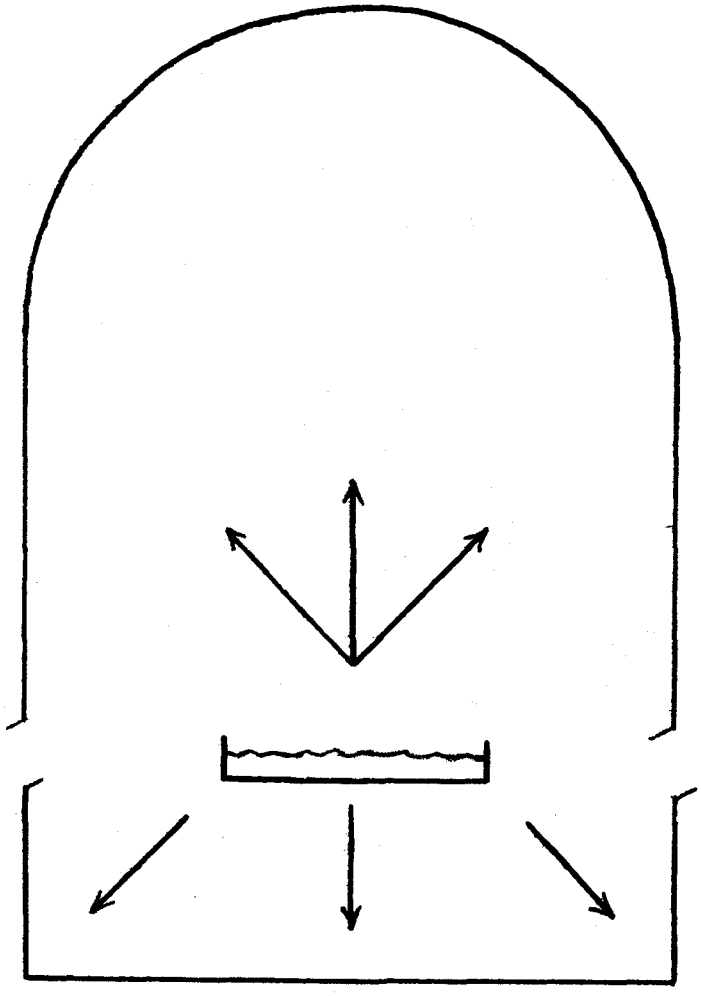

Assume: The pool radiates only to the walls
The pan radiates only to the floor

Figure 3.3 Radiation from the Suspended Pan

on any given comparison with measurement is limited to at least the variation through that element. This problem is bounded unlike the node structure problem where each time step is based upon the results of the previous one.

d) inexact properties

Many aspects of the lithium combustion add small errors which may or may not accumulate. If they do accumulate, they would add to the uncertainty in the results above, beyond the idealizations and simplifying assumptions already made. For most properties in LITFIRE (thermal conductivities, heat capacities, densities, emissivities) standard reference values are used, assuming that the test cell is constructed of standard materials. Properties of materials are most critical when they are near the combustion zone, since in that event they can affect the combustion rate extensively.

In addition to the semi-static properties, there are properties in the bulk pool and on the surface which can never be exactly modelled simply because of the complexity of the exact processes. These include non-uniform product accumulation, wicking, non-uniform emissivities, etc. They account for much of the uncertainty in the reaction rate calculation.

IV Model Development and Verification

4.1 Introduction

The tests performed at HEDL can be classified into three areas for the purpose of analysis and comparison in this report. These are: (1) tests which did not ignite (LC-1, LN-1, LN-2), (2) tests which ignited in nitrogen only (LN-3), and (3) tests which ignited in normal air (LA-1, LA-2). This categorization is very helpful in separating out individual effects which are in general strongly coupled.

The results of the comparisons helped to improve LITFIRE in two distinct areas. First, studying the differences between the predicted behavior and the experimental behavior motivated additions and changes to the model itself. Secondly, "best estimates" for the many adjustable parameters in LITFIRE (the fine tuning knobs) were obtained for these small-scale spills.

In the discussion which follows in this chapter, both of these aspects of the comparisons are described in some detail. The ordering of the text is chronologically similar to the way in which the data was actually analyzed. This should give the reader some flavor of the coupled nature of the processes in LITFIRE and the way our solutions converged to their present values through several iterations of changes. Plots are contained in the appendix which give an appreciation for the

accuracy of the code at this stage in its development. It should be emphasized when viewing these, that the error in making a "blind prediction" is likely to be higher than our observed errors having the results already in hand.

Adequate verification of LITFIRE depends upon the accuracy with which it predicts the containment response of tests like those performed at HEDL. In order to define the containment response, we looked for the critical areas in the structures and in the pool. The appended plots were chosen as the appropriate basis, including:

1) cell gas temperatures
2) steel vessel wall temperature
3) spill pan and/or lithium pool temperature

It can be shown that the cell gas pressure is primarily a function of the gas temperature (and a weaker function of the gas consumption rate), therefore the pressure is not used in our comparisons. Nevertheless, peak gas pressure is an important number for the reactor designer, so we should pay some respect before putting the issue to rest.

The HEDL tests which we analyzed showed a trend for the pressure to monotonically drop during combustion. This is a direct result of the geometry, i.e. large vessel surface area to volume ratio and no concrete insulation. It indicates that the combined effects of atmosphere depletion due to combustion and efficient cooling are sufficient to prevent overpressurization. However, our case studies of larger, concrete-covered containments indicate that overpressurization is still a problem (see also appendix page A1).

Besides temperatures and pressures, a complete verification of LITFIRE would have to include measurements of the reaction rates which form the source term. For LN-3, this is extracted readily from the reaction pan mass measurement. However, for LA-1 and LA-2 the effects of mutliple species combustion are somewhat more difficult to extract. For LA-2, we were able to compute the multiple species reaction rates from the HEDL oxygen concentration measurement; however, our results are in conflict with the reaction pan mass measurement and are therefore subject to doubt. For LA-1 we are lacking a pressure measurement, therefore no analysis was attempted for this test.

4.2 Tests with No Combustion

4.2.1 Overview

In these tests with no source term, the system simply responds passively to an initial disturbance away from equilibrium. This response is well-characterized in terms of heat transfer relations such as:

convection	$\dot{q} = h\ A\ (T_1 - T_2)$ $h\ (G_r, P_r)$	Newton's Law of Cooling Heat Transfer Coefficient	(4.1)
conduction	$\dot{q} = k\ A\ \frac{dT}{dx}$ $k\ (T)$	Fourier's Conduction Equation Thermal Conductivity	(4.2)
radiation	$\dot{q} = \sigma\ A\ (T_1^4 - T_2^4)$ σ = constant	Stephan-Boltzman Law Stephan-Boltzman Constant	(4.3)

The predictions of LITFIRE are generally quite good for these tests. The lithium temperature profiles differ somewhat in LN-1 and LN-2 due to an initial surface reaction which is quickly extinguished. The fire dies presumably because of the temperature dependence of the reaction rate and to some extent the buildup of a protective product layer.

The cell gas and steel vessel temperature profiles are modelled less accurately than the lithium pool; however, this is primarily due to the smaller absolute changes in temperature which occurred. The low heat capacity atmosphere is particularly susceptible to small variations in the nodes around it ($C_p \simeq 7$ BTU/ °F for the atmosphere, $C_p \simeq 420$ BTU/°F for the steel vessel). In addition, the steel vessel is sensitive to the ambient temperature and to the precise value for the ambient heat transfer coefficient. For these runs, absolute magnitude is a fairer comparison than percent difference. We expect that most of the errors observed for low temperature, non-ignited spills will not be important in the higher temperature spills.

Our experience with the no combustion tests has identified the following areas of sensitivity: exact knowledge of physical properties and test conditions, and non-ideal geometrical effects.

4.2.2 Physical Properties and Test Conditions

Both static and dynamic properties can have noticeable effects in the no-combustion runs. Static properties such as steel conductivity and emissivity are in principle obtainable to very high accuracy. In order to maximize the accuracy of LITFIRE, attention should be paid to using reliable values — within one or two percent. After all, the quality of the output can never exceed the quality of the input.

Dynamic properties, such as gas emissivity and pool surface properties become much more important than static properties when combustion takes place. They can vary over a range much wider than the uncertainty in static properties. Unexpectedly, the importance of dynamic properties was first observed in a no-combustion test. The pool temperature profile from LN-2 suggested that a change in pool emissivity due to the small surface reaction substantially affected the radiation heat transfer. Using a value of 0.6 for the emissivity, we obtained excellent agreement with the experimental data (see Figure 4.1). We now compute this property in LITFIRE as a function of time, assuming that a 2 mm layer of product completely covers the metallic lithium. The emissivity changes gradually from 0.2 to 0.9.

Precise test conditions are not always a source of concern, but in the no-combustion runs they stand out as did the sensitivity to static properties. The most notable example is the ambient temperature, which

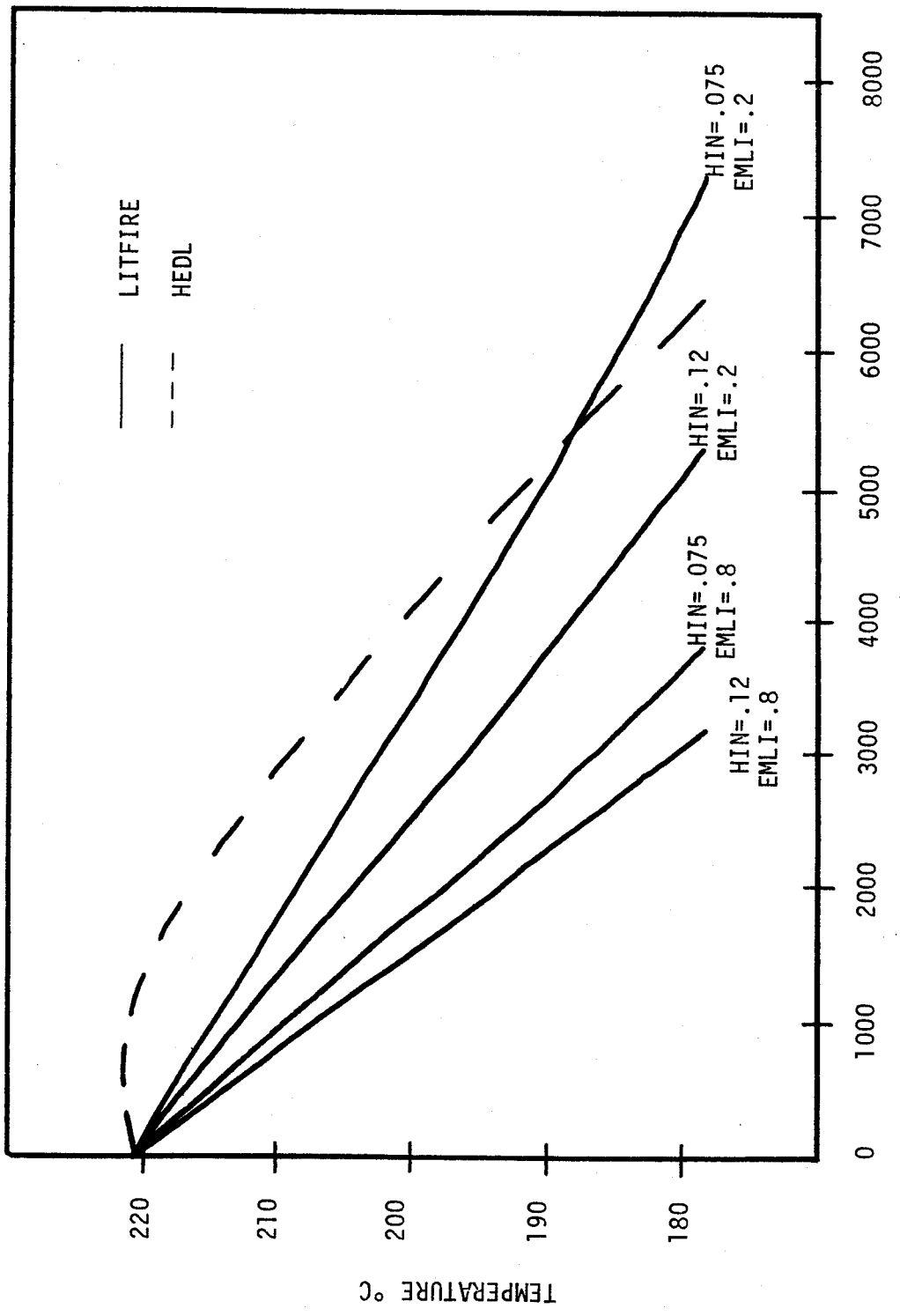

Figure 4.1 LN-1 Pool Temperature. Effect of Pool Emissivity and Convection Coefficient on Lithium Cooling Rate. HIN is the Gas Convection Coefficient and EMLI is the Lithium Pool Emissivity.

was assumed to be elevated 5 °C greater than normal in order to match the experimental results for LC-1 and LN-1. Extrapolating to larger, higher temperature spills, this type of uncertainty should disappear into the background.

4.2.3 Non-Ideal Geometrical Effects and the Determination of Heat Transfer Coefficients

Some of the processes modelled by LITFIRE require qualitative decisions and to some extent unsupported judgement. Rather than suppress that fact, we have tried to identify these areas and help the user to think about them by requiring input to the code. These "fine tuning knobs" allow flexibility in treating various heat transfer parameters, and when used properly will increase the accuracy of the code.

The best example of this is the coefficient on convection correlations for the various structures, given by

$$Nu = C\ Ra^{1/3} \tag{4.4}$$

By making C a user defined variable, the code can adapt to unusually shaped surfaces and the complicated enclosure effect. We suggest using the following values for C:

pool surface	0.12 ± .01
vertical surface inside enclosure	0.11 ± .01
vertical surface outside enclosure	0.07 ± .01
oddly shaped components inside enclosure	0.09 ± .01

We arrived at these values by trying to match all of the HEDL tests with the same consistent set of coefficients.

Transient natural convection is another geometry dependent effect which LITFIRE addresses. It is representative of a whole class of similar phenomena which reflect the fact that the oversimplified node structure of the model causes elements to respond to transients immediately and as a single entity. For solid elements, our strategy has been to use node sizes as small as possible without increasing the execution time due to either extra computations or a smaller time step. In the case of natural convection, we have added an exponential time constant to the heat and mass transfer coefficients which damps their response to abrupt changes.

The value of this time constant is to be specified by the user. Torrance and Rockett[6] suggest a correlation for the time to achieve a constant energy input rate in a cylindrical enclosure:

$$Fo = \frac{12}{\sqrt{Gr}} \qquad (4.5)$$

$$\text{for} \qquad 4x10^4 \leq Gr \leq 4x10^{10}$$

$$\text{where} \qquad Fo = \frac{\alpha \Delta t}{(\Delta x)^2} \cdot$$

The flow pattern reaches a steady state long after this, at

$$Fo \simeq \frac{40}{\sqrt{Gr}} \quad .$$

By using approximate values of α, the thermal diffusivity, and $Gr = \frac{g\beta\Delta TL^3}{\nu^2}$ we extract

$$t(sec) = 110\sqrt{\frac{L(ft)}{\Delta T(°F)}} \tag{4.6}$$

This time is very short compared to the length of the burn. However, we have continued to use this time constant with values up to 100 seconds to help smooth out the initial tendency for the combustion rate to overshoot. In other words, we have found time constants like this useful in controlling numerical instability as well as in modelling the physical phenomena.

4.3 Nitrogen Combustion

4.3.1 Overview

When combustion is taking place, the area of emphasis shifts to the so-called combustion zone, shown schematically in Figure 4.2. The principal mode for heat transfer in high temperature ignited runs is radiation, rather than convection. This case is therefore more useful in defining the dynamics of the combustion zone as well as the response of the containment to radiant heat transfer.

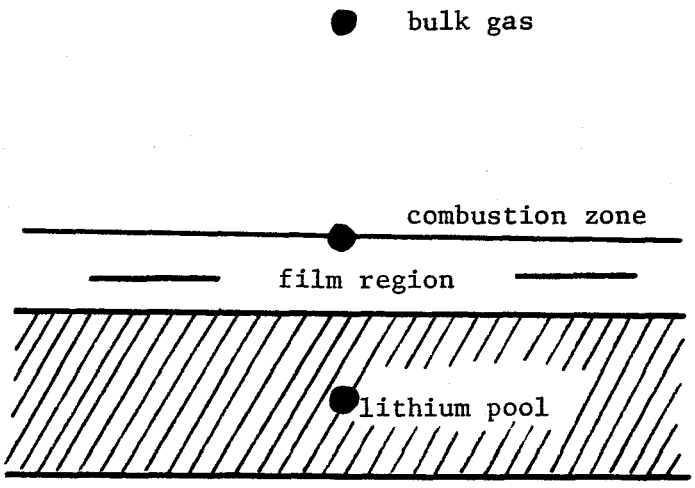

Figure 4.2 Combustion Zone Geometry

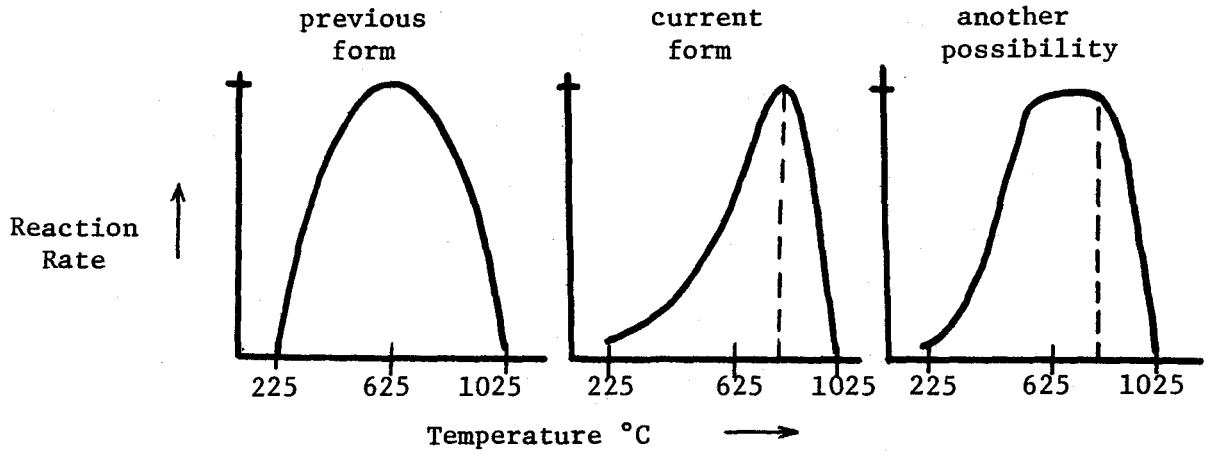

Figure 4.3 Nitrogen Reaction Rate Curves
(See Text for Explanation)

Our analysis of the LN-3 test motivated changes in the nitrogen reaction rate curve, the combustion zone emissivity, the composition of the film region, and the radiation circuit diagram. Furthermore, the gas emissivity was identified as a potential problem area.

4.3.2 Temperature Dependence of Nitrogen Reaction Rate Curve

The dependence of the nitrogen reaction rate on temperature (shown in Figure 4.3) reflects the fact that no combustion occurs below the melting point of lithium or above the point where the change in Gibb's free energy reverses sign — near 1027°C. The peak in the curve is fixed by assuming that at some point there is no hindrance and all available nitrogen combines as fast as it can reach the combustion zone. The observations from LN-2 and LN-3 suggested that the parabolic form needed to be altered to the new shape as shown in Figure 4.3.

The absence of ignition for LN-2 at a pool temperature of 530°C led to lowering the reaction rate at that temperature such that convection and radiation cooled the pool faster than combustion heated it (see calculations, p A5 of appendix). On the other end, rapid combustion near the thermochemical cutoff during LN-3 suggested that the entire curve should be pushed up in temperature. The new curve generated by these two operations is not uniquely defined; future efforts in this area may prove valuable. For example, evaluation of the correct temperature

used in these calculations remains to be seen. We have switched from using the combustion zone temperature to using the average between the combustion zone and pool temperatures, thereby raising the reaction rate. Since the combustion zone can be over 200°C hotter than the pool, this distinction has a serious impact.

The new reaction rate curve emphasizes a pathological property of tests in pure nitrogen caused by the steep slope in the high temperature regime. The fire shows a tendency to burn freely, heating the pool rapidly until the thermochemical limit is reached. This limit is generally easier to reach than the radiation heat transfer limit (i.e. where radiation balances heat production) because of the low cutoff temperature. So in most cases the temperature of the combustion zone finds itself very near 1027°C, where the reaction rate is extremely sensitive to the precise value of temperature. One result of this is that large oscillations usually occur in the combustion rate and time step as a result of small temperature changes. In addition, the length of the burn can change considerably if the code can find a way to alter the combustion zone temperature slightly. In other words, small variations in parameters can drastically affect the results.

4.3.3 Combustion Zone and Film Properties

In our early comparisons it became clear that changing the reaction rate alone could not generate lithium temperatures high enough to match

those observed experimentally. Furthermore, allowing faster combustion was only pushing the gas temperature further away from the observed values. The problem was eventually identified as poor coupling between the combustion zone and the pool — too much heat was being sent up to the cell gas and steel vessel, and too little to the pool.

A combination of two changes helped to drastically alter the temperature profiles: the film conductivity was increased to allow more conduction to the pool, and the combustion zone emissivity was reduced from 0.5 to 0.1 or less. These changes force heat down through the conduction channel as opposed to the radiation channel which generally sends most of the heat upwards (unless the pool emissivity is 1, in which case approximately equal parts radiate up and down).

Both of these modifications can be justified in terms of credible assumptions. The composition of the film region was changed from pure nitrogen to a mixture of nitrogen and lithium vapor. This thermal conductivity is then obtained from a pressure weighted mean using the known vapor pressure of lithium. This gives roughly the same order of magnitude in the high temperature range (above 1500°K), but a sizeable enhancement at lower temperatures (typical peak pool temperatures are $\sim$ 1000°C). Unlike most vapors, lithium shows an increase in thermal conductivity as the temperature decreases.[2]

Lowering of the combustion zone emissivity is in direct disagreement with the previous assumption that the flames are luminous and therefore opaque grey bodies. The assumption of luminescence is based upon the existence of macroscopic product aerosols which effectively block the line of sight from the pool. However, if one assumes that the combustion zone is very thin, as we do, then one cannot simply conclude that the combustion zone is optically thick.

Like most vapors, lithium emits primarily at its discrete rotational/vibrational lines, most of which lie between 6708 and 2302 Å. Away from these lines the vapor is essentially transparent. Ignoring for the moment the reaction products, if the combustion zone emits only at characteristic lines, then the pool should be strongly absorbing at those same lines. This implies that the combustion zone should couple well with the pool, but not necessarily with the gas. In fact, the narrow range of frequencies that are excited should lead to a fairly low averaged emissivity.

LITFIRE currently allows the user to select both the combustion zone emissivity, ε_{cz}, and the transmissivity, τ_{cz}, to pool radiation individually. We advise the use of low values for ε_{cz} ($\lesssim .1$) and fairly high values for τ_{cz} ($\gtrsim .5$). By allowing a finite transmission through the combustion zone, we had to rederive the pool radiative interchange factors based on the circuit diagram in Figure 4.4. The new heat transfer relations are as follows:

Figure 4.4

Radiation Heat Transfer

Equivalent Circuit Diagram

(modified to allow for pool emission to cell gas and structures)

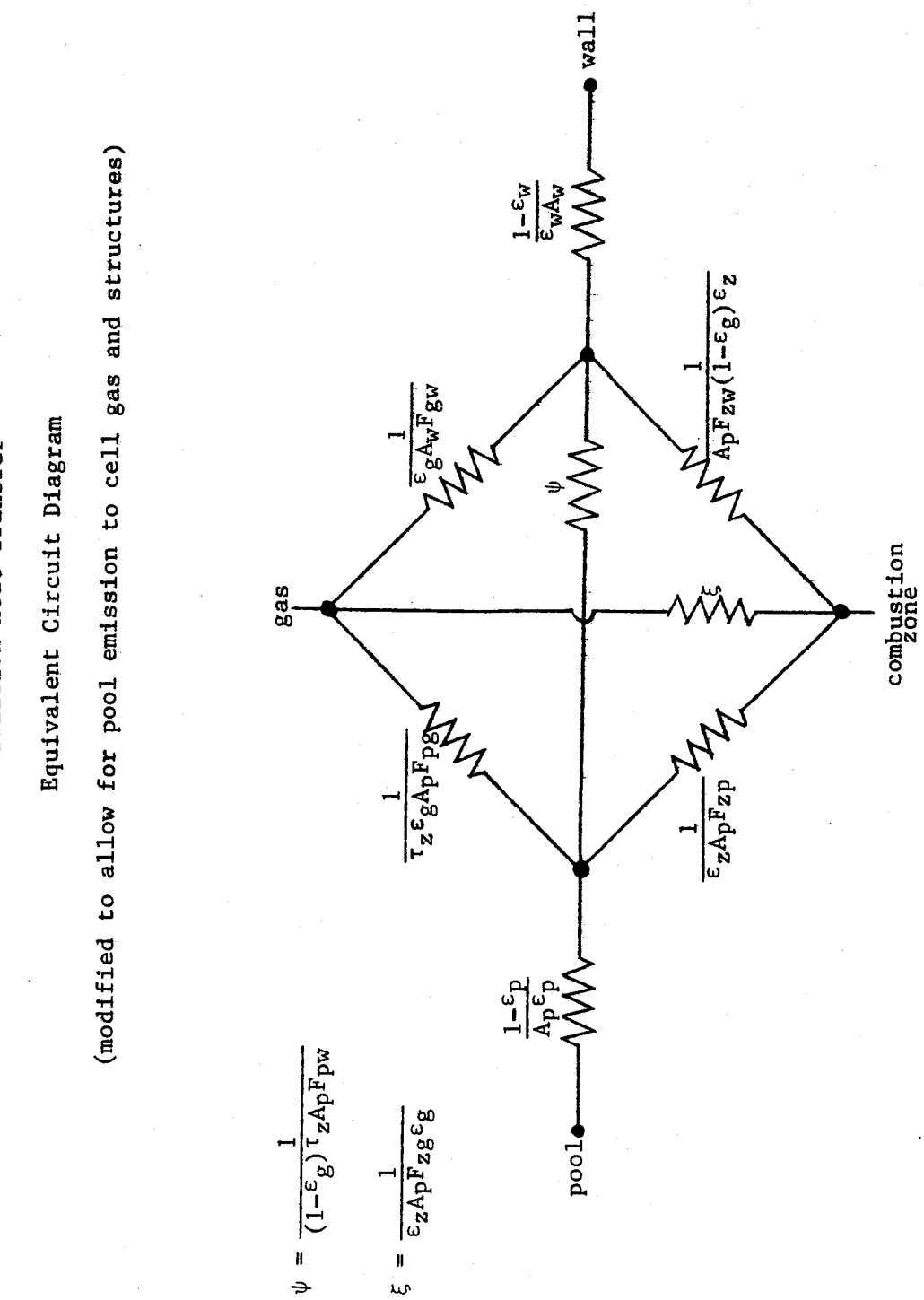

$$\text{(pool to gas)} \qquad Q_{p-g} = \frac{A_p \sigma (T_p^4 - T_g^4)}{\frac{1-\varepsilon_p}{\varepsilon_p} + \frac{1}{\tau_z \varepsilon_g F_{pg}}} \tag{4.7}$$

$$\text{(pool to wall)} \qquad Q_{p-w} = \frac{A_p \sigma (T_p^4 - T_w^4)}{\frac{1-\varepsilon_p}{\varepsilon_p} + \frac{1-\varepsilon_w}{\varepsilon_w}\frac{A_p}{A_w} + \frac{1}{(1-\varepsilon_g)\tau_z F_{pw}}} \tag{4.8}$$

where τ_z is not necessarily equal to $(1-\varepsilon_z)$. In general, $\tau_z \leq (1-\varepsilon_z)$.

Given the importance of radiation from the combustion zone, this area deserves more detailed study, particularly in defining the correct values for ε_z and τ_z. Figure 4.5 compares LITFIRE results before and after the increased coupling between the combustion zone and the pool. The latter profiles include lithium radiational cooling as detailed above, which tends to work against the coupling.

4.3.4 Mass Transport to the Combustion Zone

Based upon the observation of violent churning in the pool as well as the fact that gases are being consumed in the combustion zone, one might expect more turbulence in that region — therefore more heat and mass transfer. In fact, the vacuum left when nitrogen is solidified into Li_3N is a driving term not even considered in the LITFIRE model. This suction effect might explain the initial speed of the reaction not predicted by our model. Keep in mind though, that the temperature dependent hindrance factor on nitrogen combustion could also explain

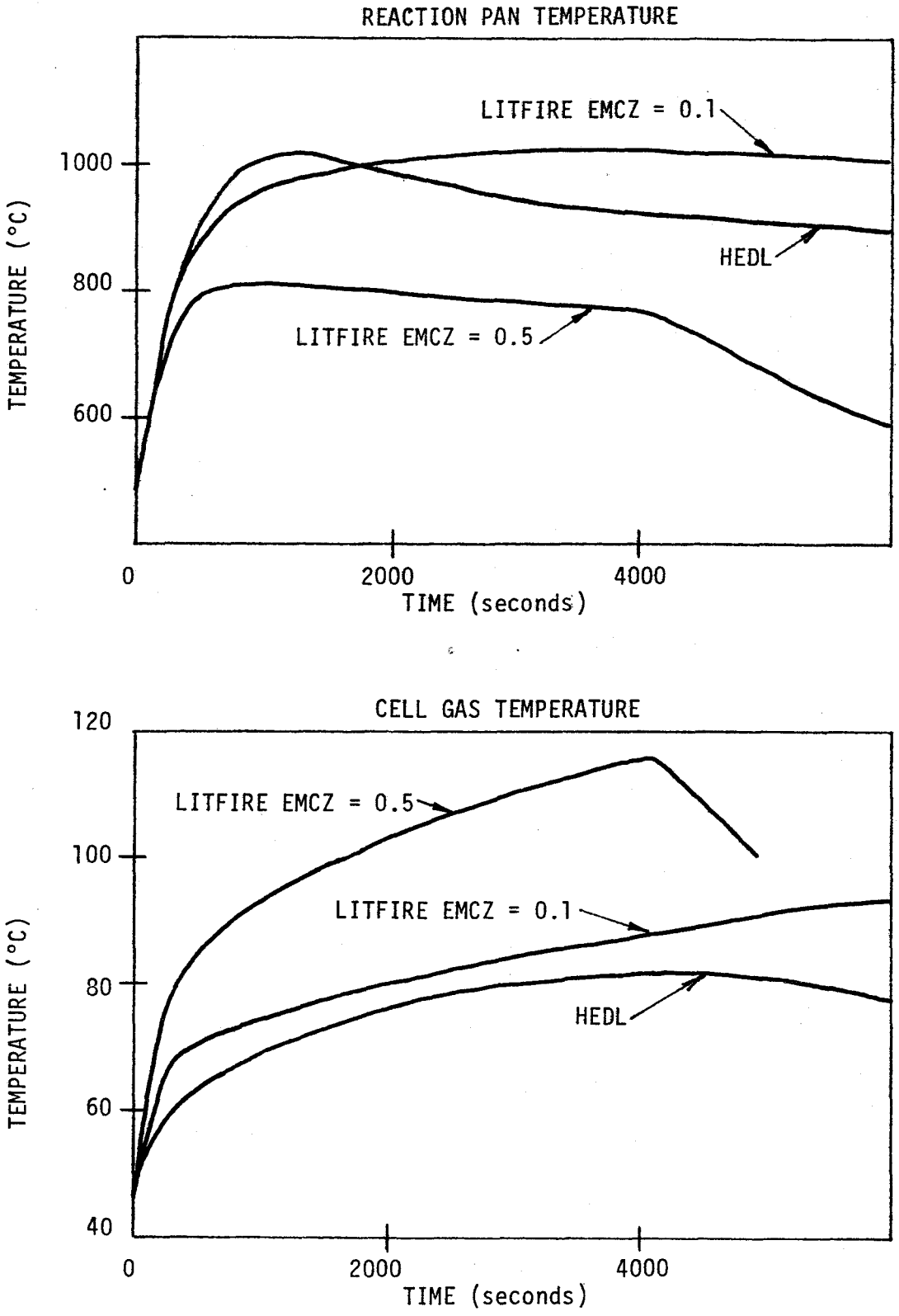

Figure 4.5 Effect of Changing the Combustion Zone Emissivity and Film Conductivity

away the discrepancy. One of the central ideas on which LITFIRE has been based is that the reaction rate is controlled by convection according to the assumption that mass diffusivity and thermal diffusivity are equal (see Figure 4.6 and also see reference 2 for discussion of mass transport).

In addition to the initial speed of the reaction, after 2000 seconds the actual rate was suppressed below the prediction, presumably due to product formation. A theory which is consistent with both of these observations has been advanced by Ostroushko, et al.[10] It is postulated that the kinetics of the lithium-nitrogen reaction are expressed very satisfactorily by the "topochemical reaction of Kolmogorov and Erofeev":

$$\alpha = 1 - \exp(-kt^n) \qquad (4.9)$$

where α is the extent of the reaction. Glancing at the experimental data confirms that the proper form is indeed roughly exponential. More work on defining k and n, as well as the coupling of this theory with theories of oxygen combustion is needed. The present estimates of the current model are a principal limitation on the accuracy of the code.

A good first guess at the problem could be formulated by multiplying the old calculation of reaction rate by an enhancement factor ϵ and an exponential decay factor $(1-\alpha)$:

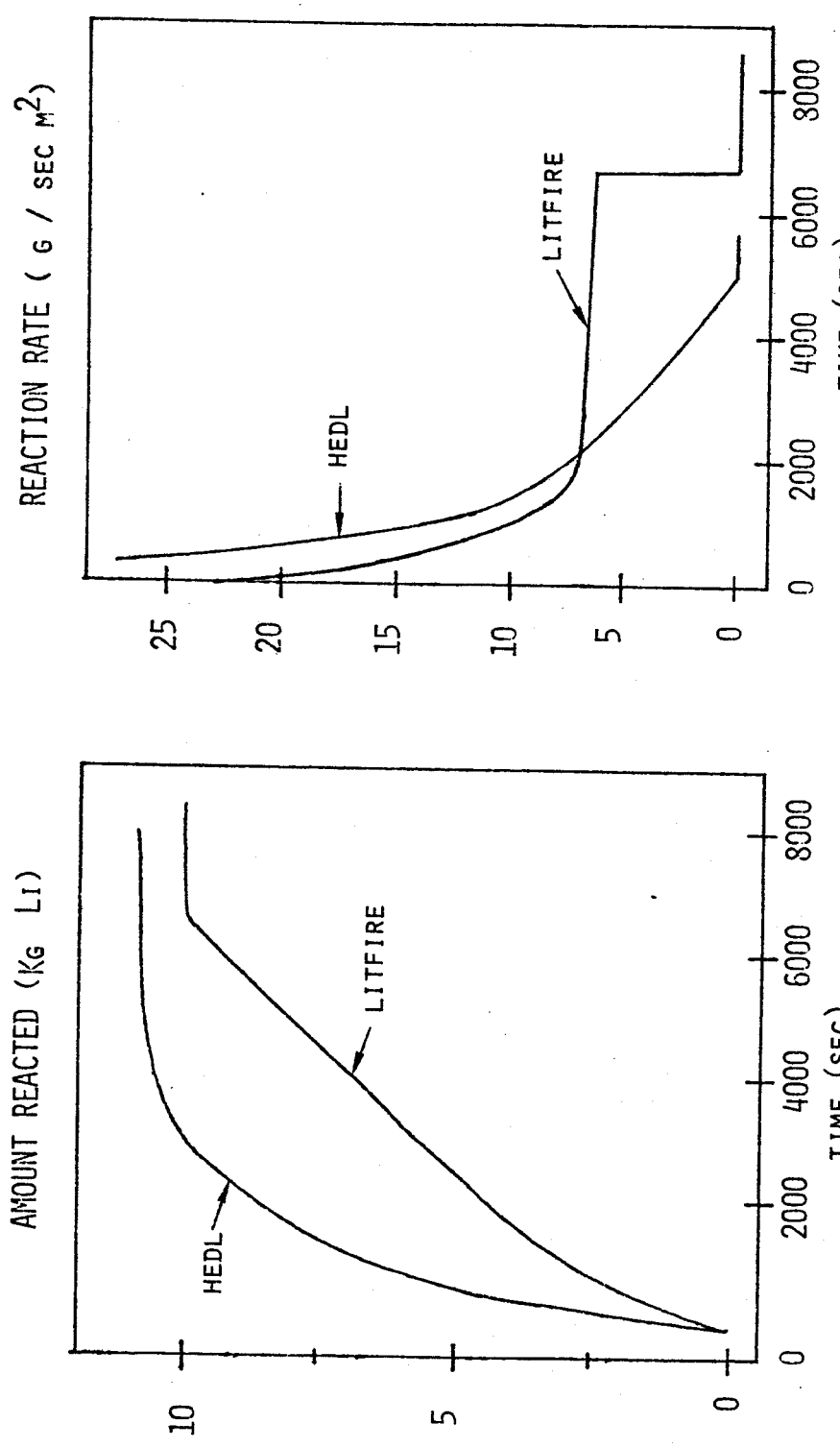

Figure 4.6 LN-3 Lithium Consumption Curves (assuming only Li_3N formed)

$$RR_{new} = \varepsilon \, RR_{old} \, (1 - \alpha) \qquad (4.10)$$

where $$\alpha = \frac{\int RR_{new} \, dt}{N}$$

and N is a normalization factor to keep α between zero and one.

4.3.5 Cell Gas Emissivity

In order to keep the cell gas from becoming unreasonably hot, we were forced to keep the gas emissivity below 0.05. After implementing the new model for the combustion zone and film described in Section 4.3.3, the effect of varying EMG has been substantially reduced. Nevertheless, since the cell gas temperature is one of the most important numbers generated it will be necessary to develop a reasonably accurate model to predict the dynamics of aerosol generation and removal. The model currently releases a fraction of the combustion products into aerosol, but has no mechanism for removal.

Figure 4.7 shows the sensitivity of the cell gas temperature using 0.1 for the combustion zone emissivity. When full species combustion is approached, a much larger amount of aerosol will be generated, making radiation to the gas an even more important effect. More discussion of this will appear in the following section.

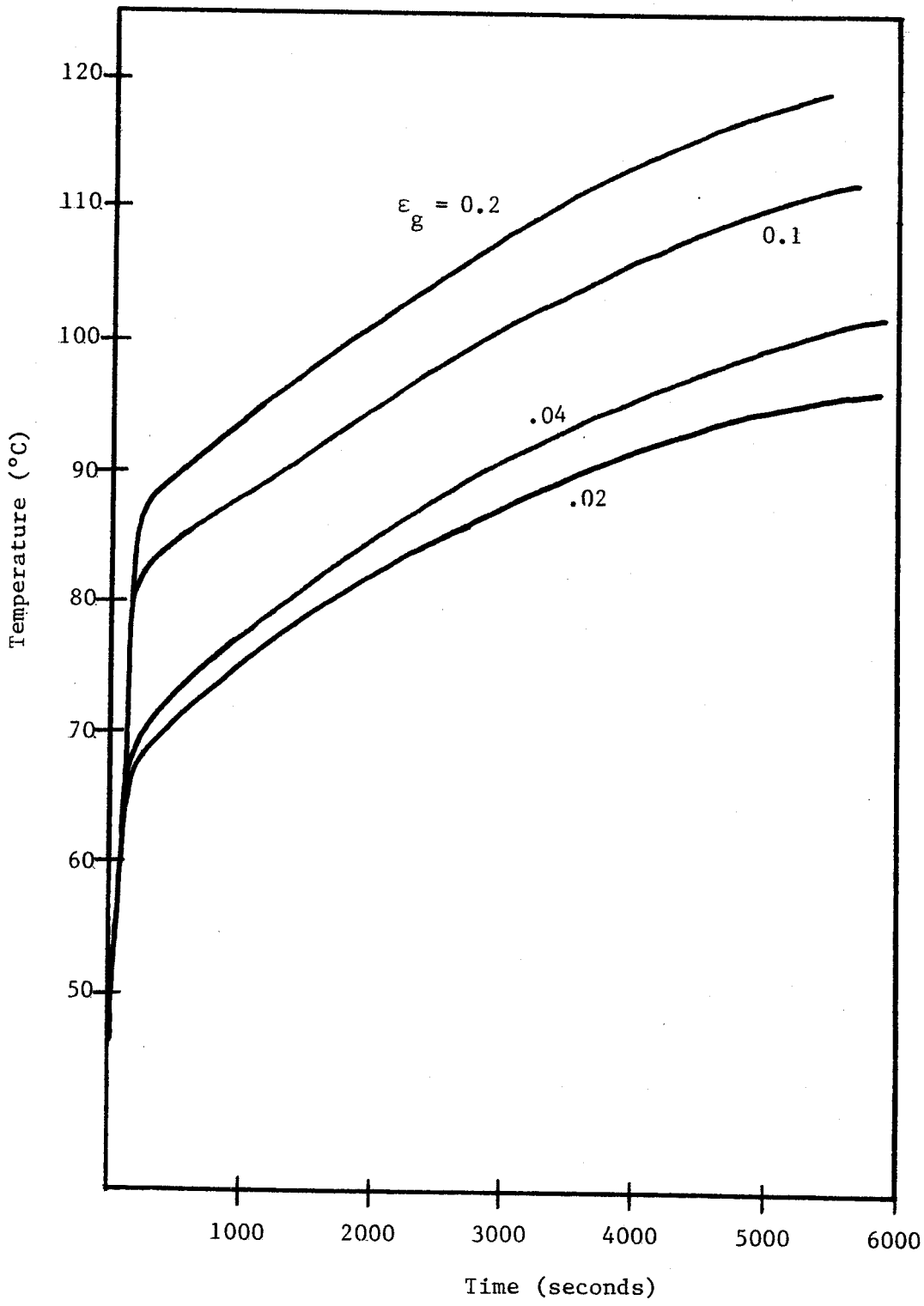

Figure 4.7 LN-3 Sensitivity of Gas Temperature to Gas Emissivity, ε_g.

4.4 Multiple Species Combustion

4.4.1 Overview

Because tests with multiple species combustion are ignited runs, the emphasis is still on the combustion zone and radiant heat transfer. Many of the effects present with LA-1 and LA-2 were already observed for LN-3. The most notable added feature is multiple species combustion kinetics.

Through analysis of the nitrogen tests, it is possible to establish — qualitatively if not quantitatively — the effect of temperature on the nitrogen reaction rate. The primary obstacle to defining this was the possible inapplicability of Reynolds's analogy for the mass transport. With oxygen now present, the effect of oxygen concentration on the nitrogen combustion rate must be included as well as both the effects of temperature and of nitrogen concentration on the oxygen combustion rate. These complications make it extremely difficult to infer precise relationships from our limited sample of data. If we further add in the fact that the oxygen concentration was not monitored continuously, and for LA-1 there is no pressure data avilable, then it becomes clear that only qualitative statements are justified in our analysis.

As observed at HEDL, the smoke generated during lithium-air combustion is mostly Li_2O, some LiOH, and virtually no Li_3N. Therefore, unlike nitrogen tests, the gas emissivity changes a great deal throughout the fire. The net result on cell gas temperature and pressure is a more pronounced effect; therefore serious consideration must be given to aerosol transport and kinetics. The nature of this topic is very complex, but the crudeness of the modelling currently in LITFIRE allows us sizeable gains even for small investments of effort. Observing the LA-1 and LA-2 profiles in the appendix, we note that LITFIRE is conservative in its estimates. So at worst we will have an upper bound which is quite acceptable. As we shall see, after remodelling the combustion zone and film region the sensitivity to gas emissivity has been reduced.

4.4.2 Some Observations on Lithium-Air Reaction Kinetics

In order to investigate the accuracy with which LITFIRE predicts combustion rates, experimentally inferred values had to be developed from the available data. Two different (independent) techniques were attempted: one involves simply differentiating the load cell output to form a gas consumption rate, the other requires application of the ideal gas law

$$PV = nRT \tag{4.11}$$

to the profiles of temperature and pressure. Figure 4.8 points out the fact that these two methods are in disagreement with one another. However,

Table 4.1

LA-2 Reaction Rate Calculation

time (seconds)	pressure mPa	temp. °K	moles O_2	moles N_2	O_2 rate moles/hr	N_2 rate moles/hr
0	.123	315.8	132.2	482.4		
120					25.65	145.35
240	.124	322.5	130.5	472.7		
420					121.2	291.1
600	.120	335.3	118.4	443.6		
1200					123.9	106.4
1800	.112	372.0	77.1	408.1		
3600					61.75	29.33
5400	.112	383.3	28.4	427.6		

[note: 62.5 moles were added at 4400 seconds]

time (seconds)	N_2 combustion rate Kg Li/hr m^2 HEDL	LITFIRE	O_2 combustion rate Kg Li/hr m^2 HEDL	LITFIRE	% O_2	pool temp. °C
120	30.27	27.88	3.56	27.15	21.35	304
420	60.64	1.80	16.84	27.68	21.1	699
1200	22.17	0.0	17.19	21.04	18.45	999
3600	6.10	0.0	8.59	4.93	11.12	982
8220	6.74	17.77	0.50	3.82	5.19	860

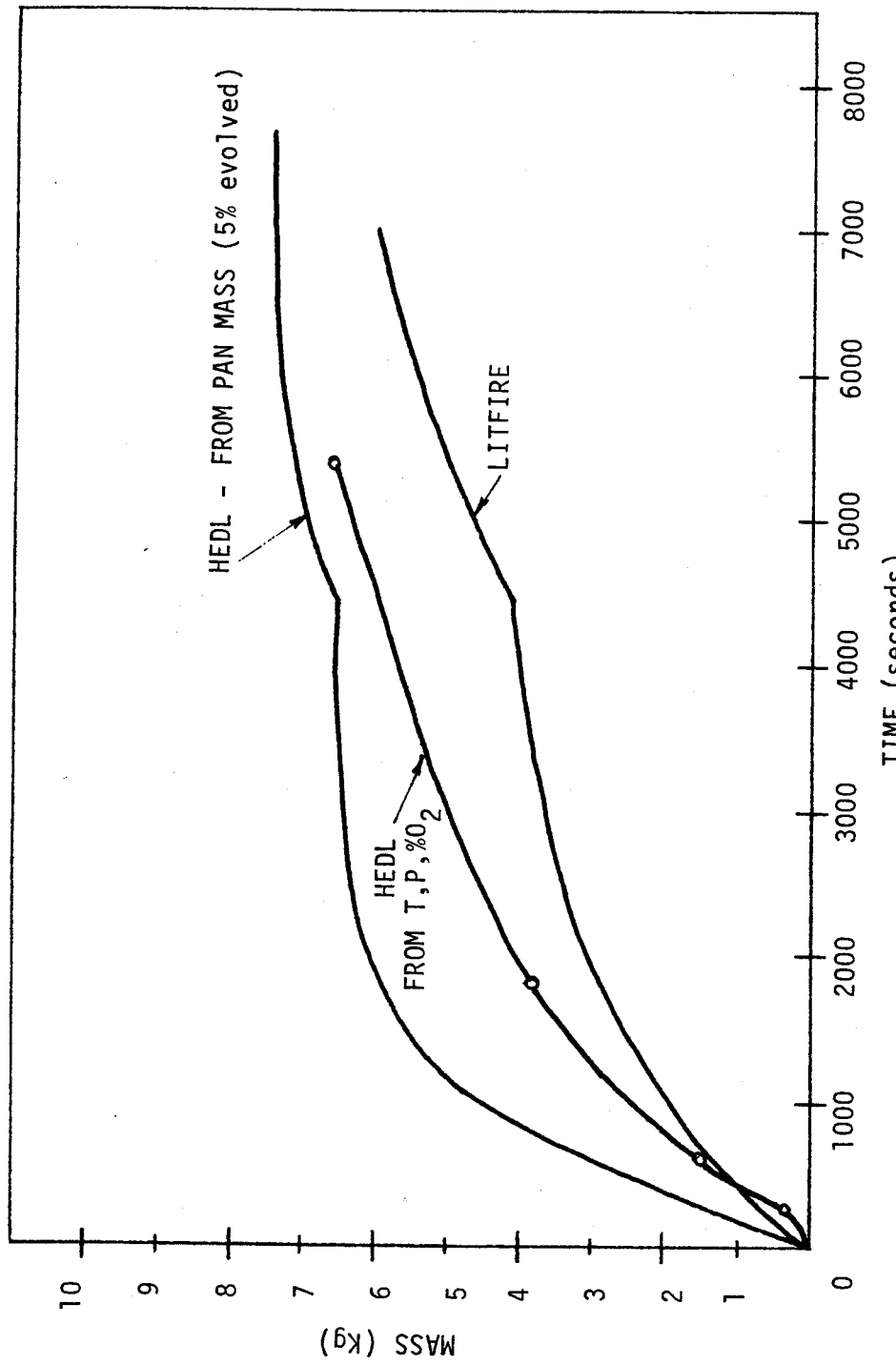

Figure 4.8 LA-2 Amount of Gases Consumed

since both curves are substantially higher than the LITFIRE prediction, if either of them is an accurate representation then we have further evidence that LITFIRE underpredicts the reaction rates. The reason for this underprediction could stem from an error in the mass diffusion calculation or from an error in the temperature and oxygen concentration dependences of the nitrogen reaction rate curve. The comparison shown in Figure 4.9 for the oxygen concentration profiles tends to support this latter conclusion. The higher values of oxygen concentration measured experimentally imply that nitrogen is not being consumed fast enough in relation to oxygen.

There are two credible explanations for this effect. Both depend upon an accurate definition of the temperature and oxygen concentration at the exact location where reactants combine. Since oxygen is not hindered from reacting the way nitrogen is, it can be presumed that the combustion zone is an oxygen-poor environment compared to the bulk gas. In calculating the nitrogen reaction rate versus oxygen concentration, the bulk values for O_2 and N_2 masses are used. This leads to over-predicting the oxygen concentration, and thus lower values of the nitrogen reaction rate.

The other possible explanation involves the large temperature gradient which exists between the combustion zone and cell gas, and also between the combustion zone and pool. If some combustion occurs outside the boundary of our idealized, infinitely thin combustion zone node, then the true temperature at the reaction site is not nearly so high as predicted. Because of the steepness of the nitrogen reaction rate

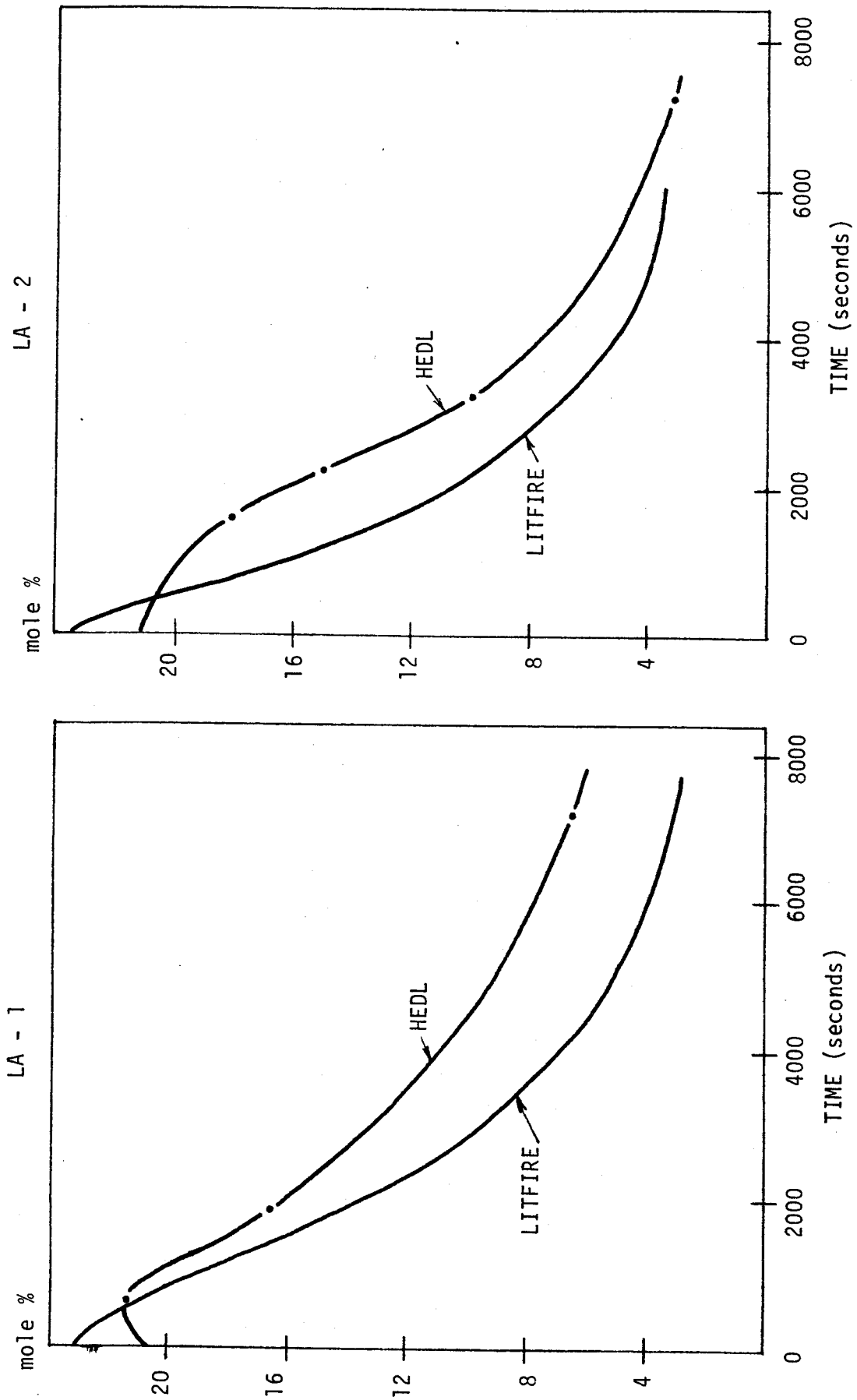

Figure 4.9 Oxygen Concentration In the Cell Atmosphere LA-1 and LA-2

curve, even small gradients could be very important. Intuitively, we might well expect that the integrity of the combustion zone boundary is not strictly upheld. Turbulent bursts of cool air are likely to mix with the flames, giving rise to combustion at lower temperatures — therefore higher nitrogen reaction rates.

Although the oxygen concentration data gives compelling evidence of miscalculating the hindrance factor for nitrogen combustion, it should be remembered that the mass diffusion calculation is still in doubt. In fact, LA-2 was even more surprising than LN-3 because the measured oxygen combustion rate was initially faster than we thought possible assuming mass to be transported in accordance with Reynolds's analogy. Unlike LN-3, where the hindrance factors could be changed to account for the difference, for LA-2 there are no hindrance factors operating on oxygen. Therefore, the underprediction of oxygen combustion can only be due to low predicted mass diffusion rates.

4.4.3 Gas Emissivity Calculation

After making the changes to the combustion zone and film region described in Section 4.3.3, the impact of the gas emissivity was substantially reduced (see Figure 4.10). Nevertheless, this area

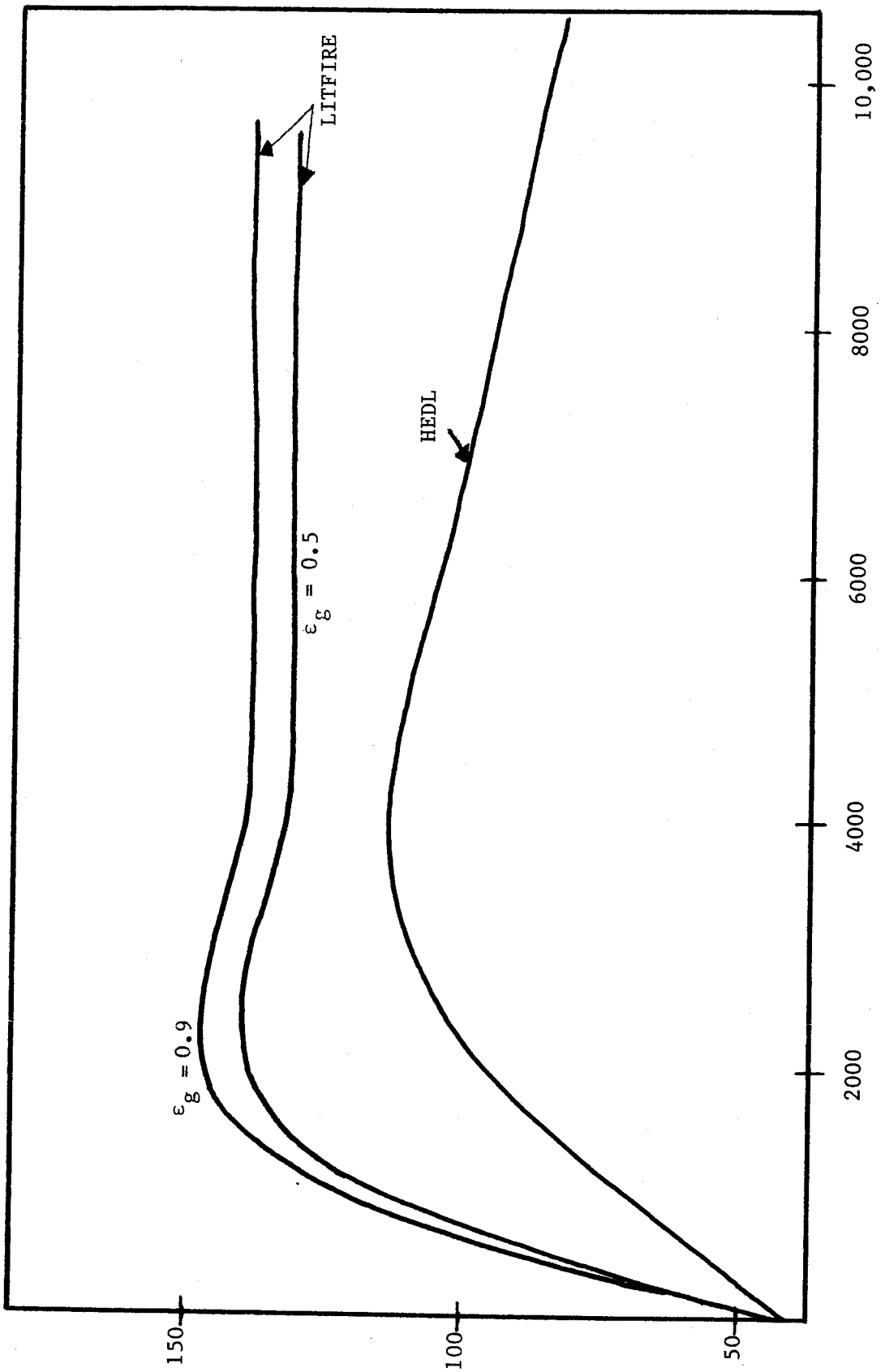

Figure 4.10 LA-2 Cell Gas Temperature Sensitivity to Gas Emissivity, ε_g.

still deserves further attention and development.

Since LITFIRE possesses no mechanism for aerosol removal, the ultimate gas emissivity is always 1 provided there is enough product evolved. It was our experience that this state was reached very quickly (at about 100 seconds) when as little as 5% of the product was released. In reality, there is a balance between production, agglomeration, and removal which may conceivably lead to ultimate emissivities lower than 1.

As usual, the simplest approach available is to define a new input parameter called the "sticking time." The sticking time is equal to the average time for an aerosol particle near the wall to be removed from the gas. In order to define "near the wall," we assume that any aerosol within an inch of the wall is subject to being removed. Then the fraction of airborne particles removed per second is equal to the fraction near the wall divided by the sticking time. The sensitivity of the results to various values for the sticking time has not been tested.

4.5 Summary of Comparisons

The major conclusions from the comparisons cited above are summarized in Table 4.2. See also Chapter VI and Table 6.1 for

more discussion of the conclusions and recommendations generated from this work.

Table 4.2

Summary of Primary Conclusions from Comparisons

A. No Combusion

1. Pool temperature is very accurately modelled.

2. Static and dynamic properties, test conditions have significant effects. Low temperature tests are not very useful in predicting the effects of combustion.

3. Extra flexibility in heat transfer correlations proved to be very useful.

B. Nitrogen Combustion

1. Reaction rate dependence on temperature altered. Further work needed.

2. Product accumulation, vacuum effect, and pool mixing have important effects on reaction rate. We suggest implementing an exponential decay rate factor proportional to remaining amount of Li.

3. Film model allowing closer coupling of pool to combustion zone has had significant effect. Radiation from flames should be explored further to define the combustion zone emissivity related parameters.

4. Gas emissivity can be an important parameter. Aerosol removal mechanism has been added.

C. Full Combustion

1. Multiple species calculation needs to be improved. Primary change is in N_2 combustion rate at high O_2 concentration and high temperature.

2. Effect of gas emissivity much lessened by application of film model.

V. LITFIRE MODEL EXTENSIONS

5.1 Introduction

The changes in geometry already described in chapters 2 and 3 were minor modifications of a pre-existing structure. The two extensions of the model described in this chapter stand apart from the rest. These major improvements were written to allow for new interactions not originally incorporated into the code. They are: lithium-concrete combustion due to failure of the steel liner, and a two-cell geometry which allows the transfer of mass and energy between two adjacent cells. Both of these are treated with the simplest possible approach which still accounts for the important processes taking place. It is hoped that in the future this skeleton will be tested and further developed.

Neither of the two concepts is new, since the CACECO code for sodium fires has had both of these options for years.[12] However, assimilating them into the LITFIRE model structure was a new idea to which the remainder of this chapter is devoted. The results presented herein are not verified with experimental data; they are only presented to compare with the original code and observe the magnitude of the effects.

5.2 Two-Cell Code

5.2.1 Motivation for Development of Two-Cell Code

There are at least two applications forseen for the two-cell version of LITFIRE. It has been suggested by some fusion power plant designers that the reactor and blanket structure be encapsulated in a small vessel separate from the steam generators and other components within the containment dome. This would constitute a mitigating influence on the potential combustion of lithium as well as an additional barrier to radiological release. If evacuated, the inner cell would aid in keeping a clean vacuum on the plasma.

By limiting the amount of combustible gases available to the fire, the high temperatures and other destructive effects of an all-out fire, may be eliminated. The two-cell code will be able to analyze both the case of a fire contained within the inner cell, as well as the case of inner containment failure and subsequent interaction with the outer cell.

The second application of the two-cell code is in analyzing the effects of pool burning within reactor components, for instance inside pipes or even the torus itself (if it is a torus, of course). This calculation will help to define the maximum temperatures to which irradiated structures may be subjected.

5.2.2. Node Structure

The configuration of the two-cell version of LITFIRE is shown schematically in Figure 5.1. The inner cell has the same node structure as the one-cell code, except for the lack of a concrete wall and the presence of a break in the steel liner which allows for the exchange between the cells. The outer cell is composed of nodes analogous to those in the inner cell, except for the lack of a lithium pool and the added presence of the concrete wall. This arrangement nearly doubles the inventory of variables in LITFIRE which must be tracked - adding to an already huge number. Fortunately though, the complexity of the code was not doubled. Only one new item of physical nature has been added; the rest of the calculations added are completely analogous to previously existing calculations.

5.2.3 Flow Rate and Energy Balance Calculations

This new element of the program computes both the leak rate between cells of the various gases and aerosols, as well as the effect of the leak on the primary and secondary cell gas node temperatures. It is assumed that the steel liner near the crack is not directly affected by the streaming gases.

The leak rate is calculated using the well-known relation for orifices,

$$\dot{m} = C_d A \sqrt{2 g_c \rho \Delta P} \qquad (5.1)$$

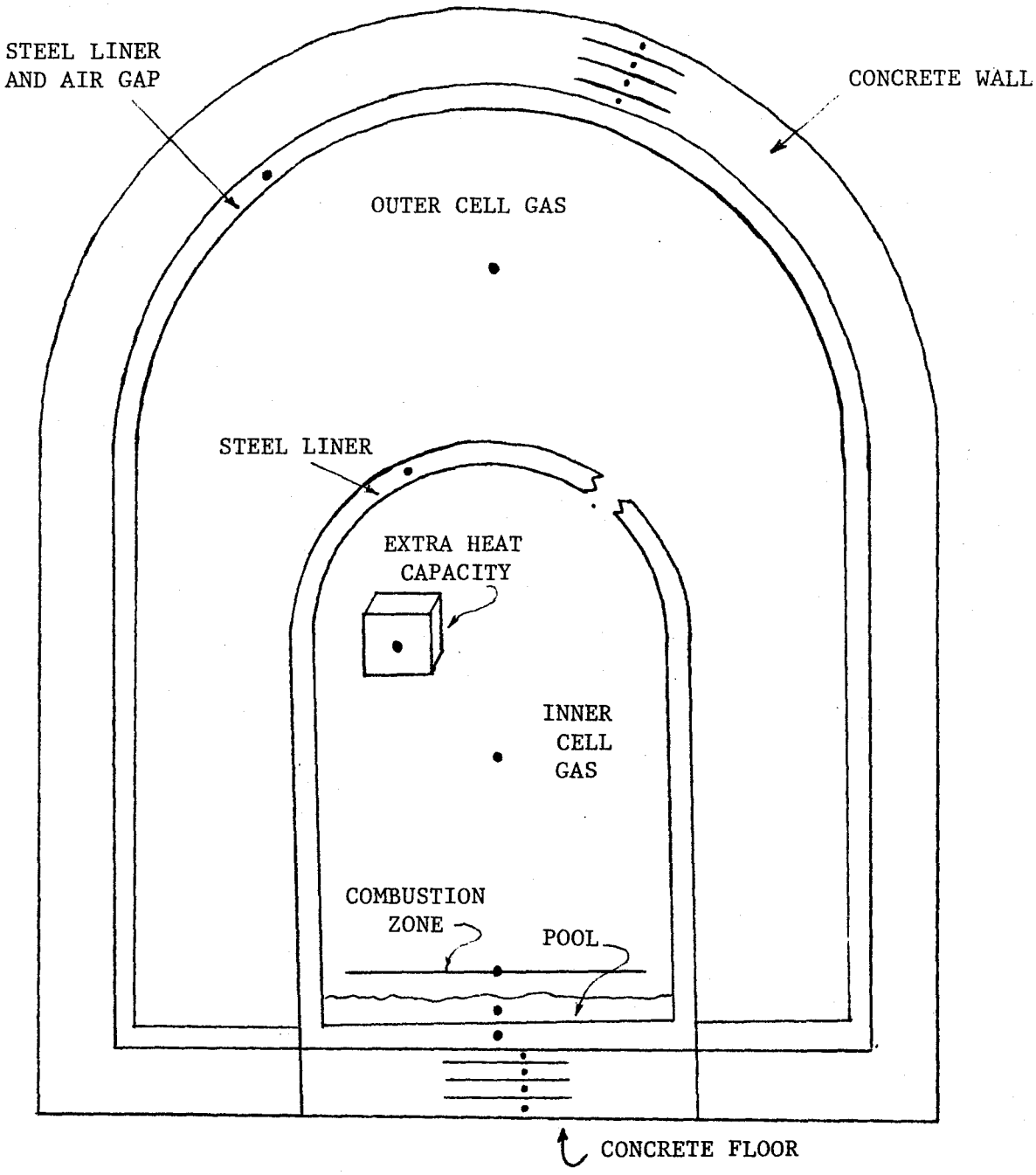

Figure 5.1 Two-Cell Node Structure.

where

$\dot{m}$ = mass flow rate

C_d = coefficient of discharge (near unity)

A = area of orifice

g_c = dimensional constant $\left(32.2 \frac{lb_m\ ft}{lb_f\ sec^2}\right)$

ρ = gas density

ΔP = pressure drop between cells

subject to the restriction that

$$\frac{P_{high}}{P_{low}} \leq \left(\frac{\gamma + 1}{2}\right)^{\frac{\gamma}{\gamma-1}} = 1.89 \text{ for air.} \qquad (5.2)$$

For larger pressure drops than this, the flow is choked and can be calculated independently of the downstream pressure. LITFIRE tracks the flow whether sonic or sub-sonic, for mass transfer either into or out of the inner cell.

The temperature changes for the primary and secondary cell gas nodes due to both the convection of gases at different temperatures and the effect of expansion or compression. Consider the energy balance equations for the system pictured in Figure 5.2. We will apply the method of forward differencing, defining $\frac{dT}{dt} = \frac{T_{n+1} - T_n}{\Delta t}$. Then,

$$\text{Final energy} = \text{initial energy} + \text{energy added}$$

$$m_{n+1} U_{n+1} = m_n U_n \pm \dot{m}\Delta t\, h_n \tag{5.3}$$

$$\left(m^{(1)} - \dot{m}\Delta t\right) C_v T_{n+1}^{(1)} = m^{(1)} C_v T_n^{(1)} - \dot{m}\Delta t\, C_p T_n^{(1)} \tag{5.4}$$

$$\left(m^{(2)} + \dot{m}\Delta t\right) C_v T_{n+1}^{(2)} = m^{(2)} C_v T_n^{(2)} + \dot{m}\Delta t\, C_p T_n^{(1)} \tag{5.5}$$

Note that the temperature dependence of the specific heats has been neglected. After algebraic manipulation we get:

$$\frac{dT^{(1)}}{dt} = \frac{\dot{m}(1-\gamma)\, T_n^{(1)}}{m^{(1)} - \dot{m}\Delta t} \tag{5.6}$$

$$\frac{dT^{(2)}}{dt} = \frac{\dot{m}\left(\gamma\, T_n^{(1)} - T_n^{(2)}\right)}{m^{(2)} + \dot{m}\Delta t} \tag{5.7}$$

where the constant γ is the ratio of specific heats C_p/C_v.

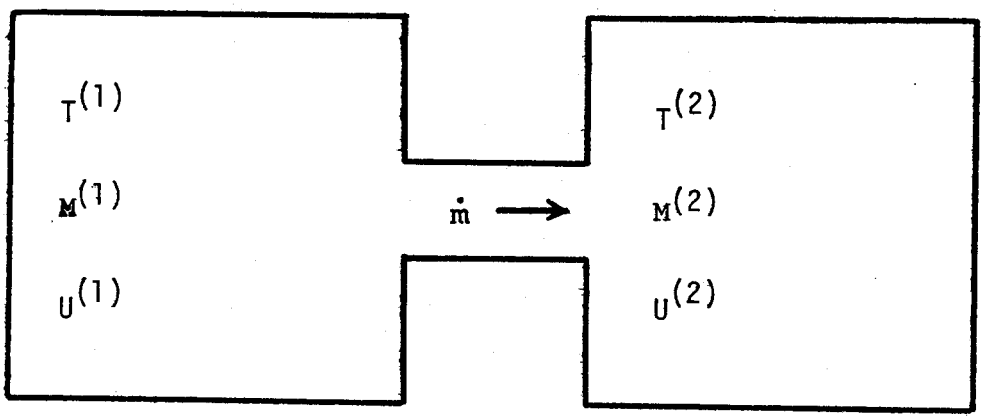

Figure 5.2 Energy Balance and Flow Rate Diagram.

These expressions allow computing new temperatures from the previous time step values, within the framework of the LITFIRE numerical scheme, which requires time rates of change to be added into the integral routine.

5.2.4 Effects of Two-cell Structure on Containment Response

The result of incorporating the two-cell calculations into LITFIRE have been analyzed by comparing a one-cell run with a two cell run without leakage. The inner cell was kept at the same dimensions in each case, but the outer cell in the two-cell run was made very large to simulate the ambient. The cell gas profiles thus generated are not exactly equivalent; the peak difference is about 4°C. This is due in part to the absence of the gas injection option in the two-cell code and in part to heating of the secondary cell not present with the one-cell run.

A more interesting comparison is between the two-cell code with no break and the two-cell code with a breach in the inner steel liner. This comparison points out the fact that compression and expansion on the cell gases can dominate the other heat transfer mechanisms. The effect of combustion is to evacuate the gases from the inner cell and to set up a flow of about 0.33 lb_m/sec from the outer cell into the inner one. Then, as can be seen on Figure 5.3, the outer cell temperature is raised by 10 °C. Also, the initial transient takes place more rapidly with the break present. The pool and other structures are affected only slightly.

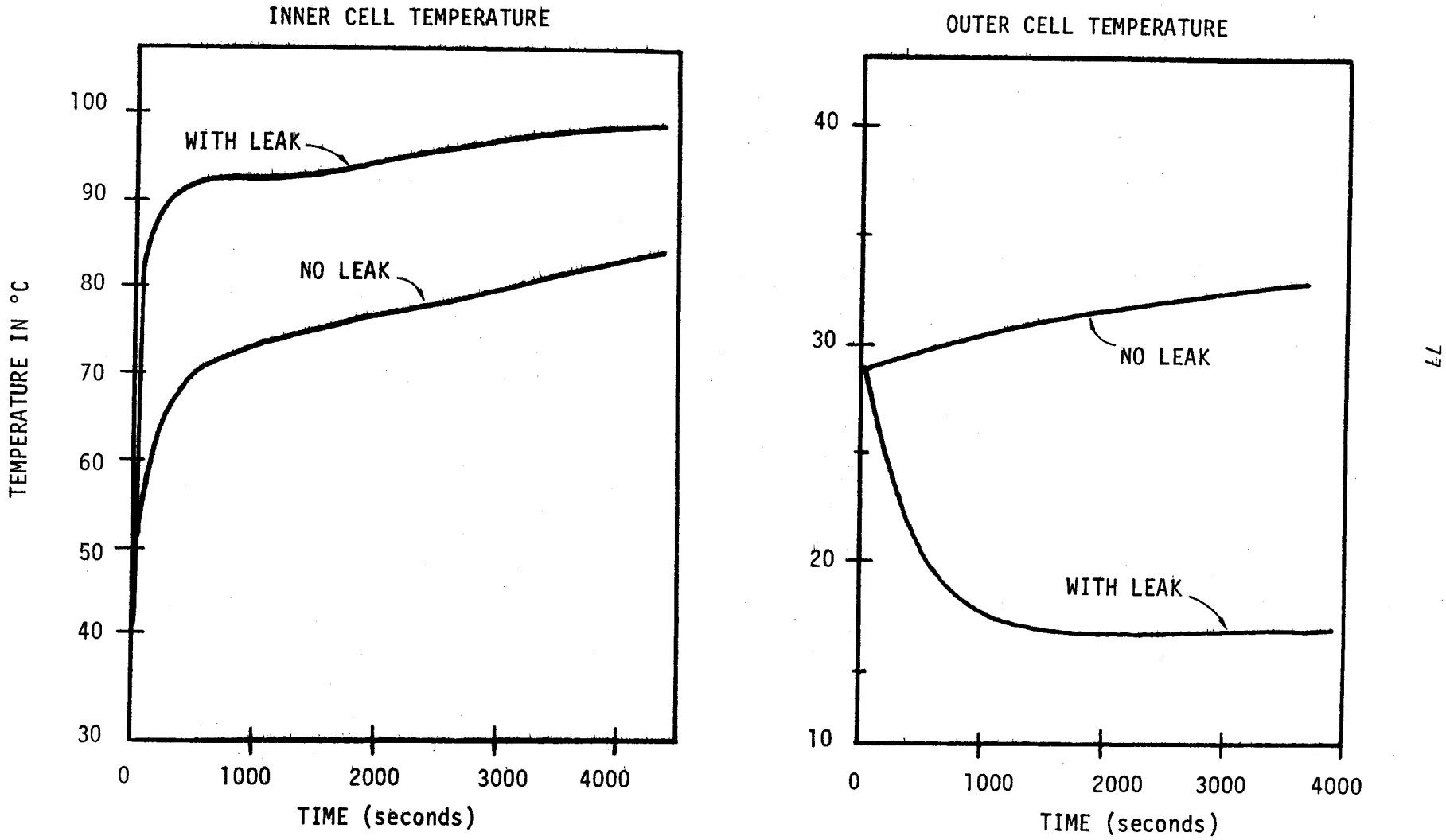

Figure 5.3 Two-Cell Results, no break vs 0.05 ft^2 break.

Even this preliminary result has significant ramifications. It states that although an intact inner cell may work to ease the consequences of a spill, if the containment fails the results may be more severe than without an inner cell. Further work is needed to ascertain the degree to which this conclusion is dependent on the volumes of the two cells and the amount of lithium involved.

5.3 CONCRETE COMBUSTION

5.3.1 Introduction

The amount of available chemical energy between lithium and concrete may be even more than for lithium-atmosphere reactions.[2] This makes the possibility of rupturing the liner and allowing contact between the concrete and lithium a very serious concern. In order to scope the possible effects of concrete combustion, we have included a primitive model of this event in the LITFIRE one-cell code. This inclusion is intended not as an accurate treatment of this problem, but only the presence of a formal structure within the code from which future improvements can be easily implemented.

The reactions occuring within the concrete have been studied by the HEDL group and by others. Some of them are listed in Table 5.1. Rather than trying to work out the details of the individual reactions, we assume for the purpose of our model that only one homogenized reaction occurs with an averaged heat of reaction equal to 150 Kcal/mole Li (or 9340 BTU/lb Li). This was calculated from HEDL data on the composition of the magnetite which they used in test LMC-1.

TABLE 5.1

Reactions of Lithium with Concrete

$8\ Li + Fe_3O_4 \rightarrow 4\ Li_2O + 3\ Fe$

$4\ Li + SiO_2 \rightarrow 2\ Li_2O + 2\ Si$

$Li + H_2O \rightarrow LiOH + 1/2\ H_2$

$2\ Li + H_2 \rightleftharpoons 2\ LiH$

$Li + LiOH \rightarrow Li_2O + \frac{1}{2}\ H_2$

$4\ Li + TiO_2 \rightarrow 2Li_2O + Ti$

$4\ Li + 3\ CO_2 \rightarrow 2Li_2CO_3 + C$

$6\ Li + Fe_2O_3 \rightarrow 3Li_2O + 2Fe$

Figure 5.4

Concrete Combustion Zone Nodalization

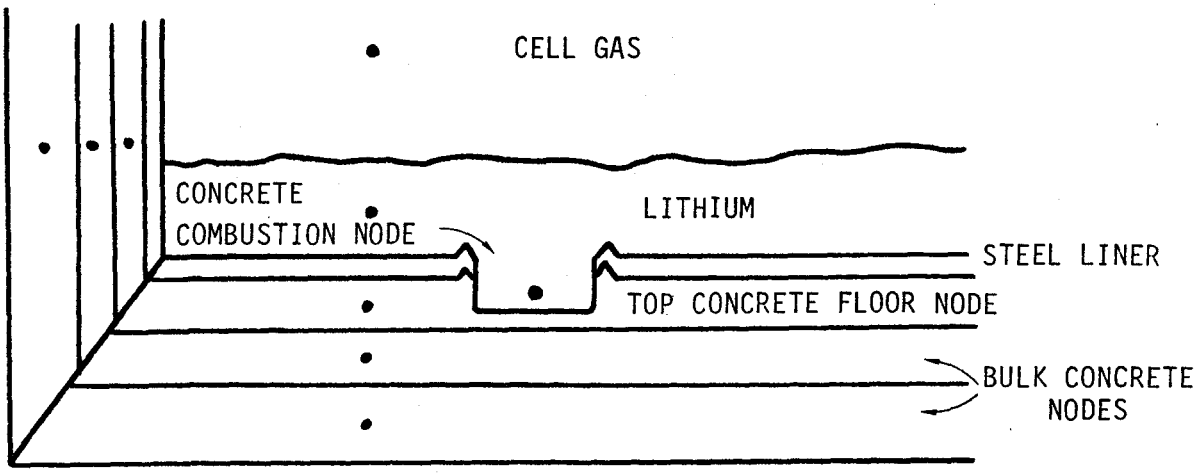

One important exception to this procedure is that water vapor combustion must be handled separately. The reaction of concrete water with lithium takes place in the concrete combustion zone as rapidly as the water is released from the top concrete node. For lack of data on release rates, we are presently using empirical data on the equilibrium amount of water present, and then imposing an exponential time constant to determine the rate. The data was taken at Argonne National Laboratory [1] and analyzed with curve fitting to give:

$$W = W_{max}\left\{1 - \exp\ 26.207 + T\ - .0721 + T\left(6.96 \times 10^{-5} - T\ (2.26 \times 10^{-8})\right)\ /\ 11.7\right\} \quad (5.8)$$

where W is in the amount of water ultimately released at temperature T in degrees Rankine, and W_{max} = 5.32 Kg.

During the HEDL concrete combustion tests it was noted that not only was water vapor released from the heated concrete, but it was probably the Li + H_2O and 2 Li + H_2 reactions which formed the proper environment for the concrete itself to ignite. This explains the five hour delay observed during the lithium - magnetite test LMC-1 before the sample finally ignited. In order to model this late ignition, we imposed the condition on the concrete top node that $T \geq 250$ °C for combustion.

5.3.2 Assumptions Made in Modelling the Concrete Combustion Zone

The extended node structure is shown schematically in figure 5.4 for reference. In modelling the concrete combustion, we made the following set of assumptions:

(a) For simplicity, we force the concrete combustion zone to be always much smaller than the concrete top node. This keeps the combustion node from interacting with the lower concrete nodes and also ensures that the properties of the top concrete node are perturbed only slightly.

(b) The heat produced in the concrete combustion node leaves only by conduction to the lithium pool and to the concrete top node. Except for hydrogen, the reaction products are confined to the concrete combustion node - consistant with the observation at HEDL that the major product was Li_2O. The hydrogen evolved does not affect the cell gas temperature, so we must add the restriction that the amount of H_2 released is small compared with the bulk cell gas mass.

(c) Water vapor is released from the concrete top node in accordance with its temperature, and from that node only. Each H_2O molecule released

gets reacted in the concrete combustion node. For every water molecule reacted, one H_2 molecule is sent up to the cell gas pursuant to the reaction $2\ Li + H_2O \rightarrow Li_2O + H_2\uparrow$. The reaction $2\ Li + H_2 \rightleftarrows 2\ LiH$ is ignored.

(d) Both the penetration rate through the concrete top node and the reaction interface area are kept constant. The physical properties of the concrete combustion node are the same as unreacted concrete. The only parameter that changes is the thickness of this node.

The concrete combustion zone is unique in contrast to the lithium/air combustion zone. First, its heat capacity is not small like that of the air combustion zone. This together with the constant penetration rate should remove all of the instability which plagues the pool surface. Second, the reaction with concrete does not depend upon the presence of combustible gases or their convection rate. This means that the only mechanisms for stopping the reaction once started will be the consumption of all the lithium or cooling below the ignition temperature.

5.3.3 Sample Results

After writing the changes for concrete combustion into LITFIRE, the new option was tested by executing a sample run. The input parameters are nominally those for LA-2, except that the geometry cannot include a suspended pan if concrete combustion is to take place. In addition to the geometry change, the pool depth is increased to add some thermal inertia so that pool boiling would not occur. This not being sufficient, we also decreased the cell oxygen content to 10% and decreased the concrete water content to 5 lbs/ft^3. These values are not provided here as best estimates, but simply to facilitate testing the new model. The results of this run show ignition of the concrete at 19 seconds into the burn due to contact heating with the lithium pool. The reaction rate is down an order of magnitude from that of lithium-air reactions; however before 500 seconds, the concrete combustion zone has reached 980°C - 340°C hotter than the pool. This reflects the fact that the concrete combustion zone is so well insulated.

At 550 seconds into the burn, the concrete top node begins to release water as a result of conduction from the pool (through the steel liner) and also as a result of heating from the concrete combustion zone. The release rate of water gives rise to a reaction rate of about 2 kg/hr — comparable to that of lithium-air reactions. This was sufficient to heat the concrete combustion node to 4250°C at 2500 seconds. Radiation from the pool was just enough to maintain the lithium below the boiling point. Figure 5.5 contains temperature

profiles out to 2 hours including pool, concrete top node, and concrete combustion zone. Although combustion did not cease until 5.6 hours, peak temperatures occurred in the first two hours of the test.

The results of this sample run are preliminary and do not constitute verification of the concrete combustion option. However, the effects which we observed showed that, as was expected, the consequences of concrete combustion are a very serious concern. Local and/or bulk boiling of the lithium pool as well as production of substantial quantities of hydrogen may be encountered ($\sim$6600 liters per ft^3 of concrete involved).

In order to equip LITFIRE to analyze the burning of concrete more accurately, we will need a better definition of the water release rate, as this is probably the most crucial quantity in predicting the consequences. In addition, the ability to deal with evaporating lithium should be incorporated into the model. Because lithium vapor will readily combine as it is released, the impact of pool boiling could be very severe.

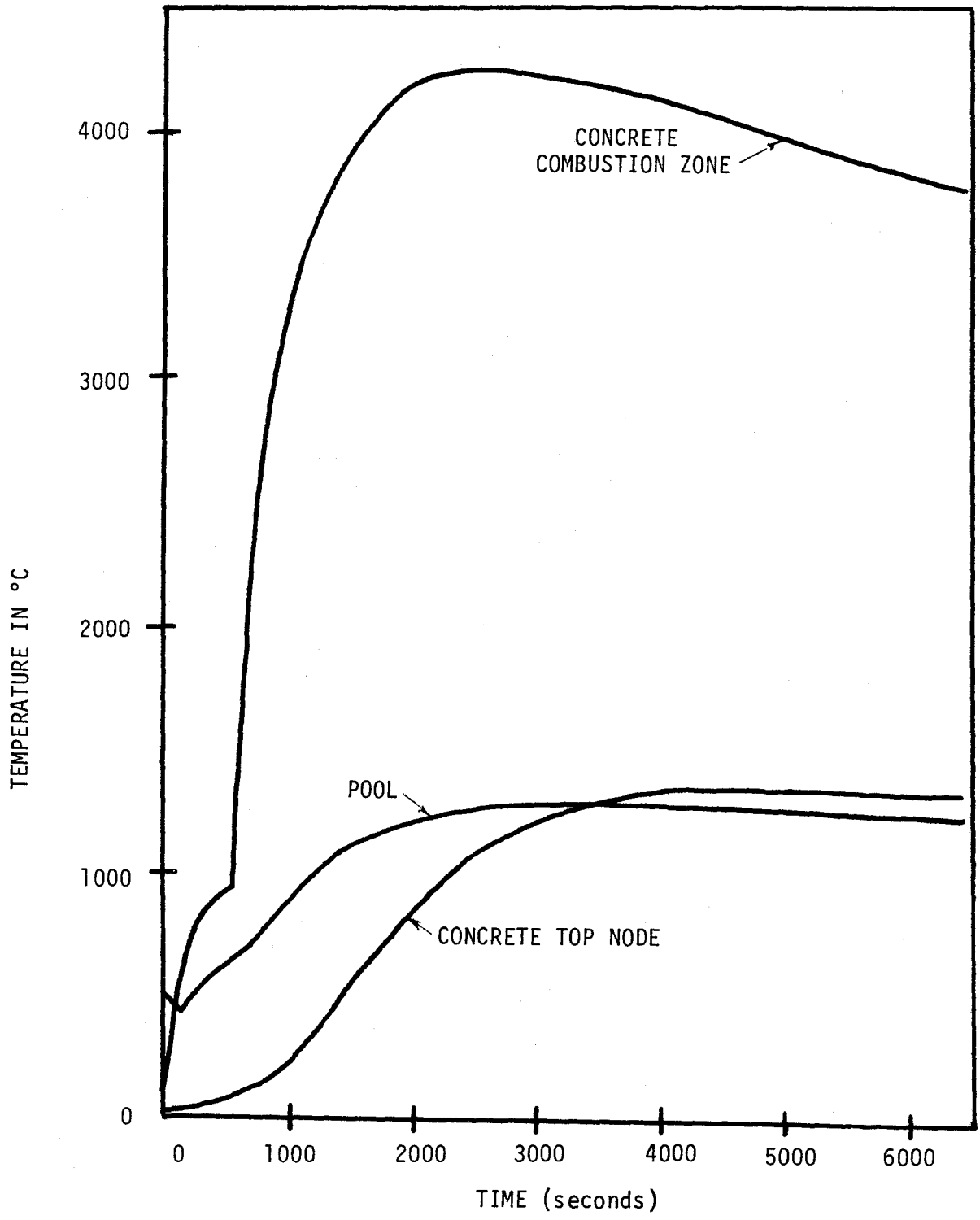

Figure 5.5 Temperature Predictions for Lithium-Concrete Reactions

VI Conclusions, Evaluations, and Recommendations

6.1 Updated Predictions for UWMAK-III

The many changes which have been made to improve LITFIRE were described in Chapter IV. These changes have allowed for closer matching of the experimental data taken at HEDL. But the true purpose of this modelling effort is to predict the consequences in a full-size, realistic reactor containment. Therefore it is appropriate to take a close look at a conceptual reactor design which was analyzed before this work, comparing current predictions with the previous ones.

In Figure 6.1 a comparison is shown using UWMAK-III as the test case with a spill equal to one full coolant loop. The results show, as was hoped, that the previous estimates were on the conservative side. The fact that the new predictions are not widely different provide a degree of confidence that the changes made to accomodate the small-scale experiment have not detracted from the ability of LITFIRE to describe full-scale spills.

6.2 The Future of LITFIRE

The success of LITFIRE to predict within 30% the results obtained at HEDL is encouraging, but certainly not conclusive. The experimental data

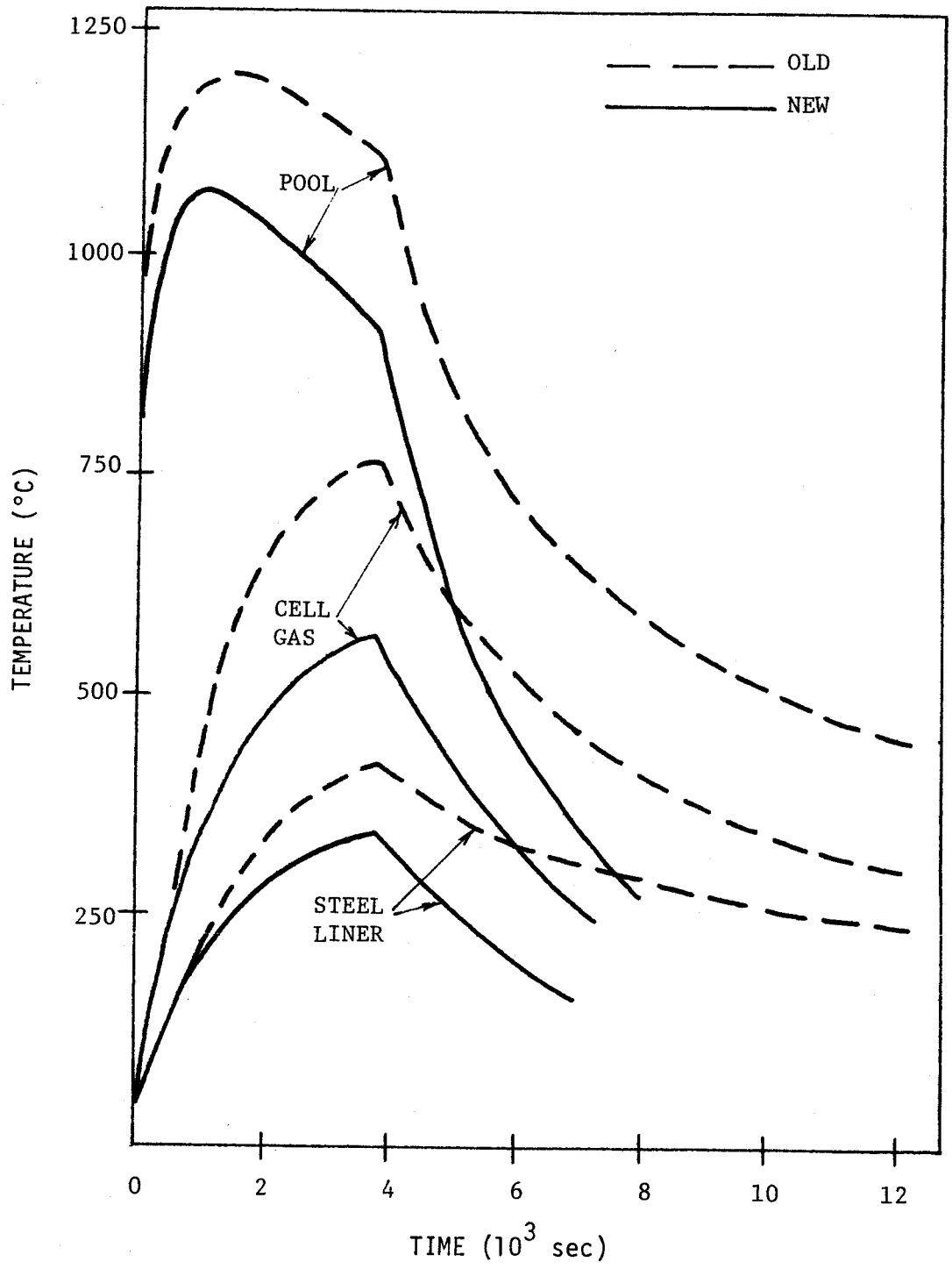

Figure 6.1 Comparison of Current LITFIRE Predictions with July 1978 Predictions Reported in Ref. [2].

base is so limited that the changes made to the model can be justly evaluated only on the basis of future experiments. It was our philosophy to use the HEDL tests primarily for pointing out areas of concern; the resolution of these problem areas will demand more experimental data and more detailed study (see Table 6.1).

Since the combustion rates are of such fundamental importance and are so poorly understood, we suggest that future experiments attempt to measure the relevant quantities involved. These include temperature and oxygen concentration near the combustion zone as well as a reliable measure of the gas consumption rate. More theoretical work is needed in this area to define the proper nitrogen hindrance factor and to account for product accumulation and suction effects on the mass transfer rates.

In the area of combustion zone and pool radiation properties, both analytical and experimental work are needed to define the energy transport rates. This involved research on the nature of liquid metal flames to determine their composition, and their emission and transmission spectra. The related problem of cell gas emissivity is probably best answered by a simple experiment measuring the radiation intensity from a black-body located somewhere in the cell.

Further verification of the concrete combustion and two-cell capabilities will be needed now that LITFIRE treats these two options.

For concrete, the most critical parameter seems to be the water release rate. To support the determination of this parameter, a general understanding of the cracking and water migration properties of concrete will be necessary. For the two-cell option, there is little or no experimental data for lithium combustion. When data becomes available, the most interesting parameters to compare will be cell gas temperatures and pressures.

As far as the computer program itself is concerned, the programming structure of LITFIRE leaves extensive room for improvement. Because of the way in which LITFIRE evolved through a series of after-the-fact additions, there is some incoherence in the coding. Since the LITFIRE program is expected to be further developed and applied in fusion safety studies, a reorganization of the program flow should be considered.

Table 6.1

Parameters Requiring Further Definition

Problem Area	Measurement or Calculation Needed
Reaction Rate:	
Mass Diffusion Rate Effect of Product Accumulation Nitrogen Hindrance Factors (vs. Temperature and O_2 Concentration)	Accurate measurement of gas consumption rates, temperature and oxygen concentration near flames
Pool and Flame Properties:	
Pool Emissivity with Product Formation Flame Emissivity and Transmissivity	Determination of flame composition and radiation properties of flames
Cell Gas Properties:	
Gas Emissivity Transient Effects on Natural Circulation Heat Transfer in Enclosures	Direct measurement Literature review
Coding Improvements:	
Change Units to SI Modularize Stucture Include Ability to Evaporate Lithium	none
Concrete Combustion:	
Water Release Rates from Concrete	
Two-Cell Geometry:	
Effect on Cell Gas Temperatures of various sized cracks	Cell gas temperatures and pressures

References

1. A. J. Impink, Jr., and W. G. Homeyer, "Tritium Regeneration in Proposed Fusion Power Reactors," Transactions of the American Nuclear Society, 5(1):100, June 1962.

2. D. A. Dube and M. S. Kazimi, "Analysis of Design Strategies for Mitigating the Consequences of Lithium Fire Within Containment of Controlled Thermonuclear Reactors," MITNE-219, July 1978.

3. R. W. Sawdye and M. S. Kazimi, "Application of Probabilistic Consequence Analysis to the Assessment of Potential Radiological Hazards of Fusion Reactors," MITNE-220, July 1978.

4. I. Charak and L. W. Pearson, "SPOOL-FIRE: Analysis of Spray and Pool Na Fire," Argonne National Laboratory, October 1976 (presented at the ANS International Meeting on Fast Reactor Safety and Related Physics in Chicago).

5. D. W. Jeppson, "Interactions of Liquid Lithium with Various Atmospheres, Concretes, and Insulating Materials; and Filtration of Lithium Aerosols," HEDL-TME 79-7 UC 20, June 1979.

6. K. E. Torrance and J. A. Rockett, "Numerical Study of Natural Convection in an Enclosure with Localized Heating from Below - Creeping Flow to the Onset of Laminar Instability," J. Fluid Mechanics vol 36 part 1, 1969.

7. Rohsenow and Choi. Heat, Mass, and Momentum Transfer, Prentice-Hall Inc., 1961.

8. Hottel and Sarofim. Radiative Transfer, McGraw Hill, 1967.

9. W. H. McAdams. Heat Transmission, McGraw Hill, 1954.

10. Ostrouska, et al, "Lithium, Its Chemistry and Technology," AEC-tr-4940, Moscow 1960.

11. N. B. Vargaftik. Tables on the Thermophysical Properties of Liquids and Gases, Hemisphere Publishing Corporation, 1975.

12. Roy D. Peak, "Caceco: A Containment Analysis Code - User's Guide," Westinghouse - Hanford Engineering Development Laboratory (preliminary report).

13. D. G. Jacobs, "Sources of Tritium and its Behavior Upon Release to the Environment," USAEC Division of Technical Information ORNL TID-24635, 1968.

Appendix

Calculation of Cell Gas Pressurization

It is shown here that in the HEDL tests, particle removal has a much lesser effect on the gas pressure than the heat of reaction. This implies that the observed underpressures were made possible largely due to efficient heat removal through the liner. Defining the following quantities:

- R = reaction rate (lb moles gas/hr)
- T = temperature of gas (°R)
- P = pressure of gas (psi)
- H = heat removal rate from cell (BTU/hr)
- K = energy production rate (BTU/lb mole gas consumed)
- n = lb moles of gas in cell
- M = atomic weight of air (lb/lb mole)
- c_v = air specific heat (BTU/lb °R)
- Mnc_p = heat capacity (BTU/°R)
- KR = rate of energy addition (BTU/hr)
- $KR-H$ = rate of energy accumulation in gas (BTU/hr)

we can derive

$$\frac{1}{P}\frac{dP}{dt} = \frac{1}{n}\frac{dn}{dt} + \frac{1}{T}\frac{dT}{dt} = \frac{-R}{n} + \frac{KR-H}{Mnc_vT} \quad .$$

We get pressurization when

$$\frac{dp}{dt} > 0 \quad , \text{ or}$$

$$\underset{①}{KR} > \underset{②}{H} + \underset{③}{MRc_vT}$$

1 - heating effect
2 - cooling effect
3 - particle removal

For an order of magnitude estimate, use the approximate values:

$H \approx 2.5$ ($^{BTU}/_{hr\ ft^2\ °F}$) 200 (ft^2) 80 (°F) = 40,000 $^{BTU}/_{hr}$

$KR \approx 4080$ ($^{BTU}/_{lb\ Li}$) 10 ($^{lb\ Li}/_{hr}$) = 40,800 $^{BTU}/_{hr}$ for LN-3

$Mc_vRT \approx .1725$ ($^{BTU}/_{lb\ °R}$) 700 (°R) 10 ($^{lb\ Li}/_{hr}$)/1.5 ($^{lb\ Li}/_{lb\ N_2}$

= 805 $^{BTU}/_{hr}$

Another technique we could use to make the point involves a comparison of the incremental pressure change due to the adiabatic reaction of one pound of nitrogen.

A. increase due to energy input at atmospheric pressure and room temperature:

$$\Delta P = n\ k\ \Delta T$$

$$\Delta T = 4080\ (^{BTU}/_{lb\ Li})\ 1.487\ (^{lb\ Li}/_{lb\ N_2})/mc_v$$

using m = 39 lbs

and n k = .032 $^{psi}/_{°R}$

$$\Delta P = 28.86\ ^{psi}/_{lb\ N_2}$$

B. decrease due to consumption

$$\Delta P = 14.7 \text{ psi} \qquad \frac{1}{39} = .377 \text{ psi}$$

We have shown that without energy removal, the effect of combustion in this temperature and pressure range would tend strongly toward pressurization.

RN2 — Reaction Rate Considerations

Although we are not able to specify completely the temperature dependence of the nitrogen reaction rate, there are a few points which we can fix. For instance,

1) lithium freezes at 900°R

   RN2 (900°R) = 0

2) Li_3N dissociates at 2340°R

   RN2 (2340°R) = 0

3) For LN-3, we observed experimentally lithium temperatures up to 2260°R. This confirms that the hindrance curve must be very steep if RN2 is to be zero at combustion zone temperature = 2300°R.

4) The absence of ignition for LN-2 allows us to fix an upper limit on RN2 at 1460°R. We do an energy balance using the data obtained from run number 031079-2:

TLI = 1460°R	RCMBN = 1.487
TS = 544°R	HF = .0341 ft/sec
HB = $.4\times10^{-3}$ BTU/sec ft^2 °R	RIFCZP = .233 (initially)
RHOA = .0782 lb_m/ft^3	RIFCZW = .5
QCN = 4080 BTU/lb_m Li	SIGMA = 4.76×10^{-13} (BTU/sec ft^2 °R^4

$Q_{rad} = .5\ (TCZ^4 - TS^4) + .233\ (TCZ^4 - TLI^4) = 2.12$ BTU/ft^2 sec

$Q_{conv} = 916\ (.4 \times 10^{-3}) = .366$ BTU/ft^2 sec

Q_{source} = (QCN) (HF) (RHOA) (RCMBN)(RN2)

then, setting $Q_{source} \leq Q_{rad} + Q_{conv}$

$$RN2\ (1460°R) \leq 0.154$$

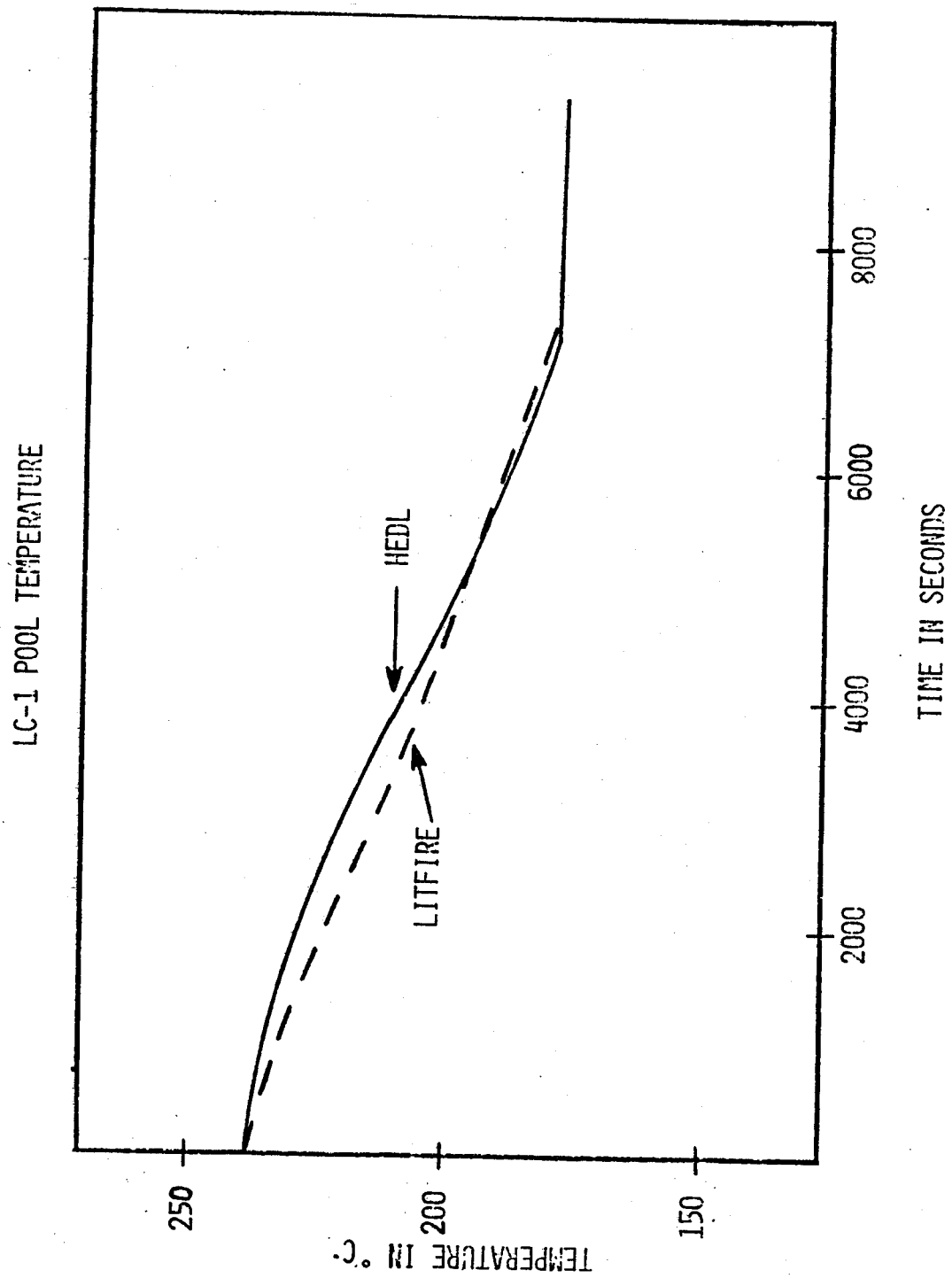
LC-1 POOL TEMPERATURE
HEDL
LITFIRE
250
200
150
TEMPERATURE IN °C
2000
4000
6000
8000
TIME IN SECONDS

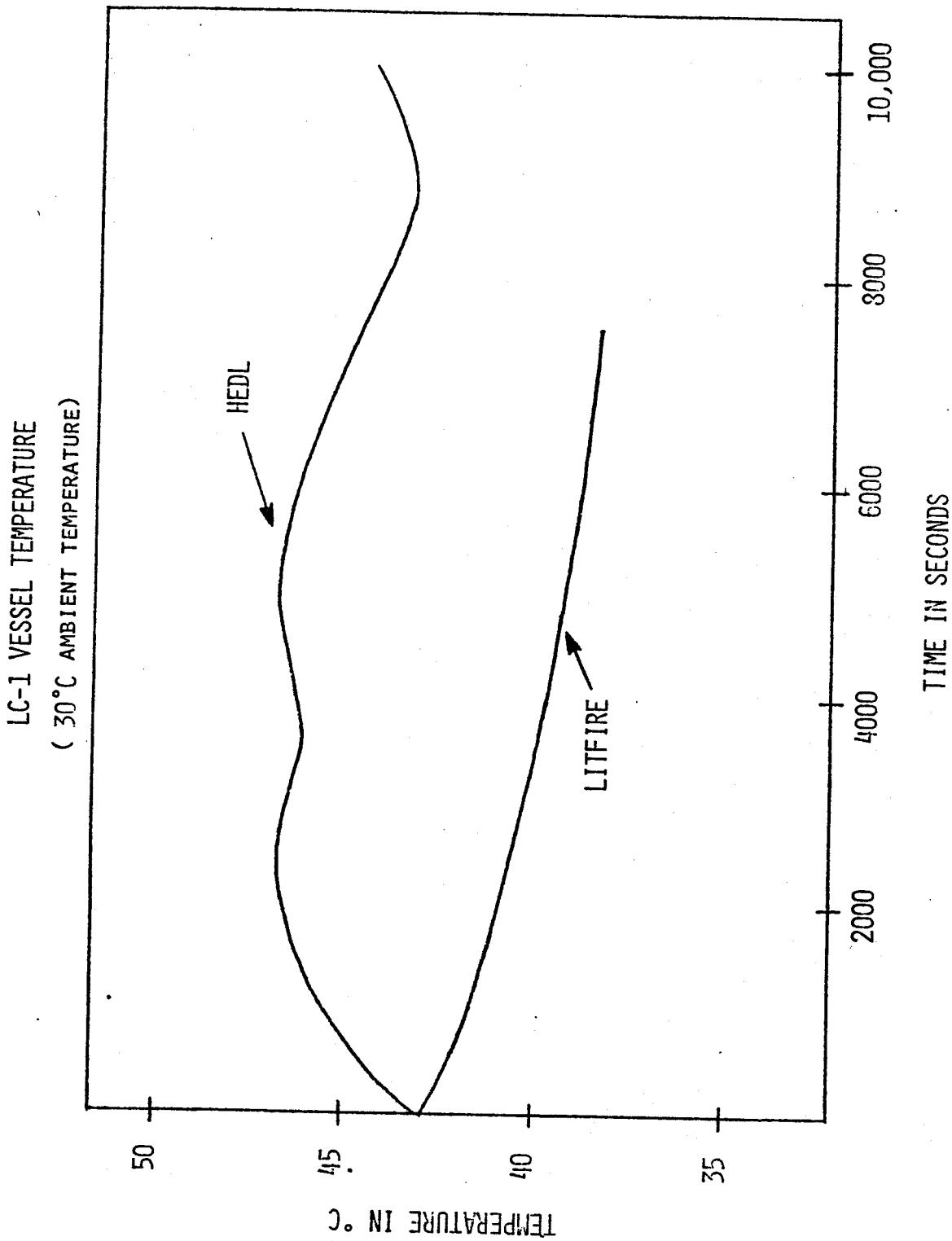
LC-1 VESSEL TEMPERATURE
(30°C AMBIENT TEMPERATURE)
HEDL
LITFIRE
50
45
40
35
TEMPERATURE IN °C
2000
4000
6000
8000
10,000
TIME IN SECONDS

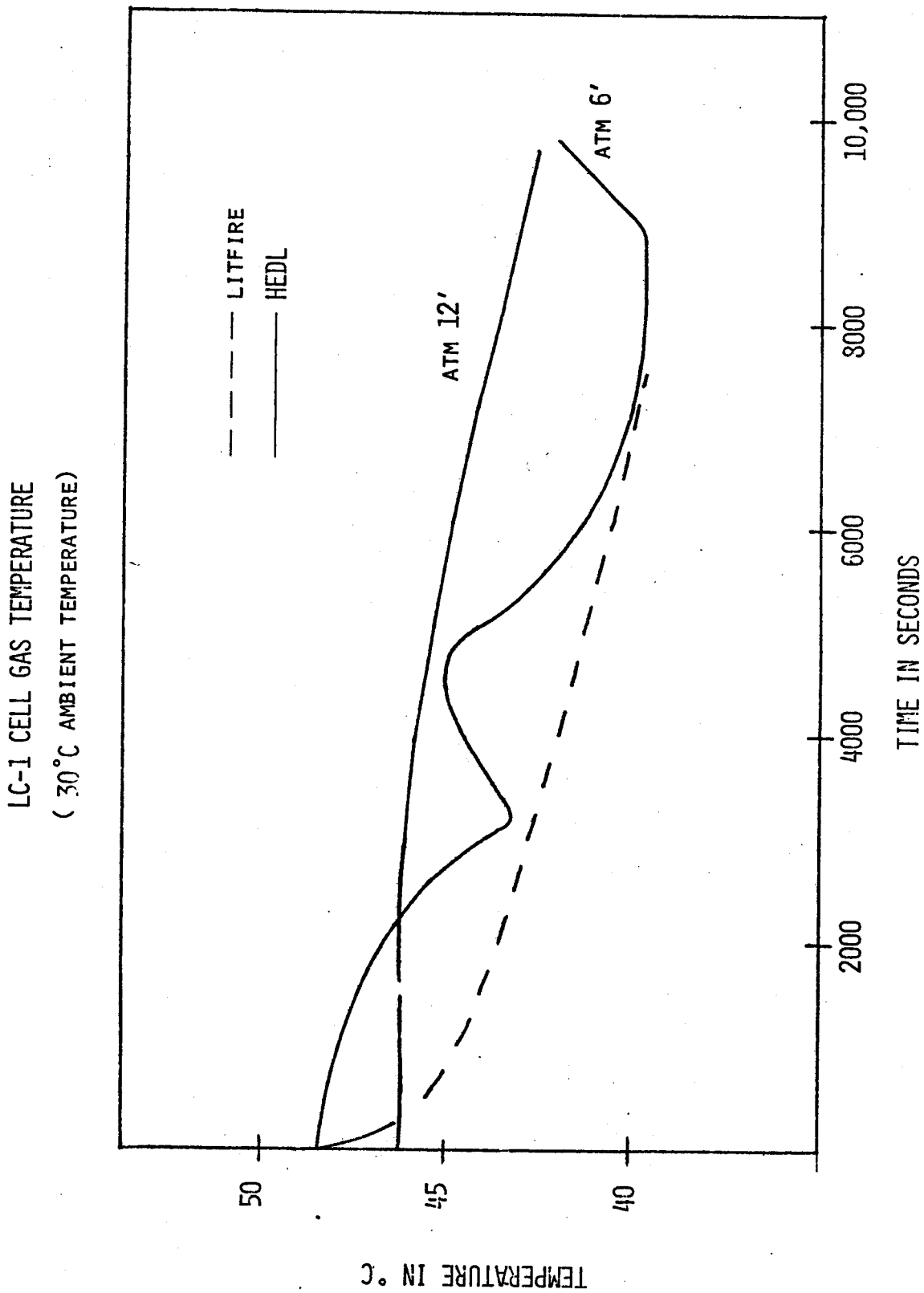
LC-1 CELL GAS TEMPERATURE
(30°C AMBIENT TEMPERATURE)
LITFIRE
HEDL
ATM 12'
ATM 6'
50
45
40
TEMPERATURE IN °C
2000
4000
6000
8000
10,000
TIME IN SECONDS

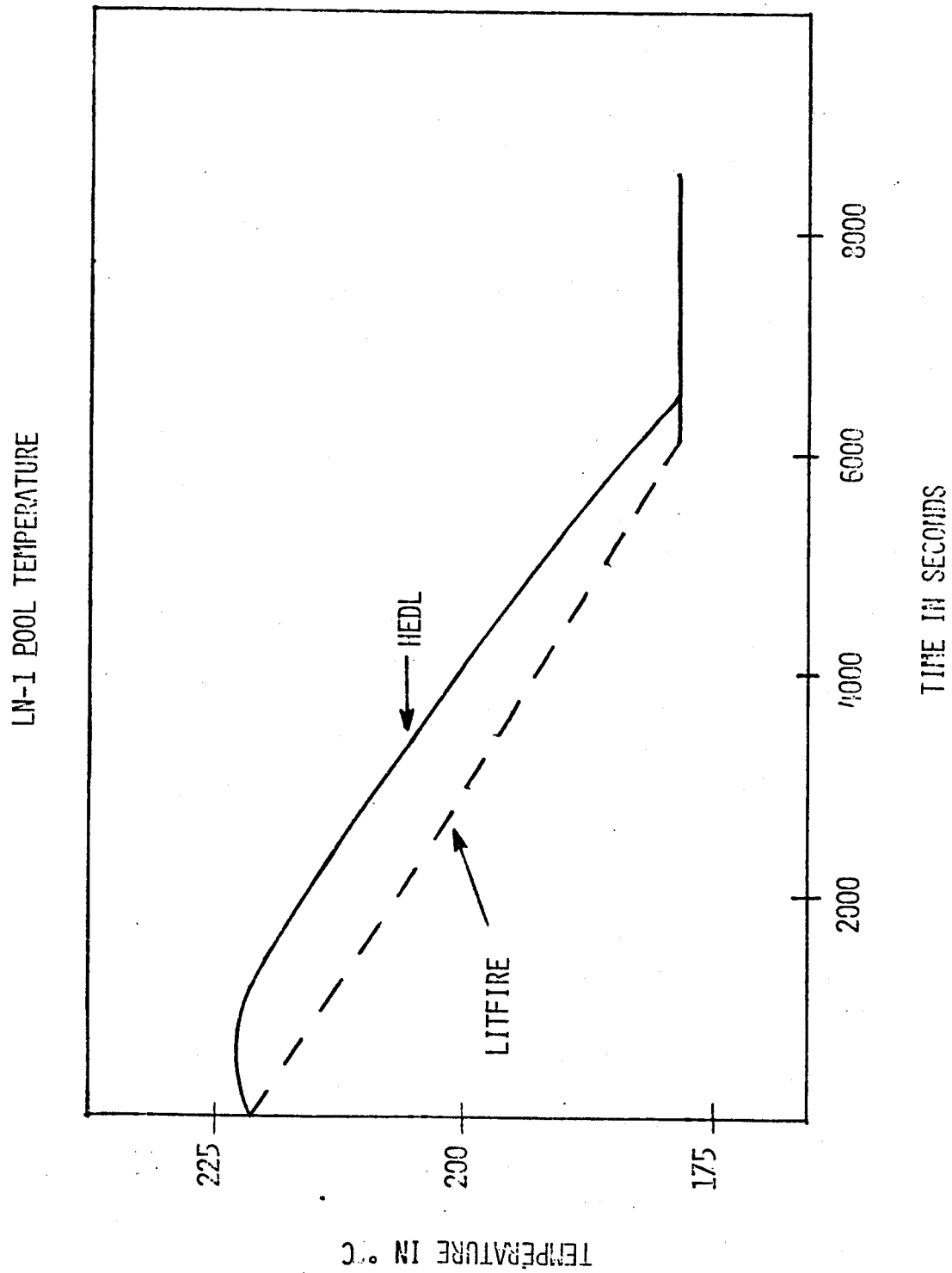
LN-1 POOL TEMPERATURE
HEDL
LITFIRE
225
200
175
TEMPERATURE IN °C
2000
4000
6000
8000
TIME IN SECONDS

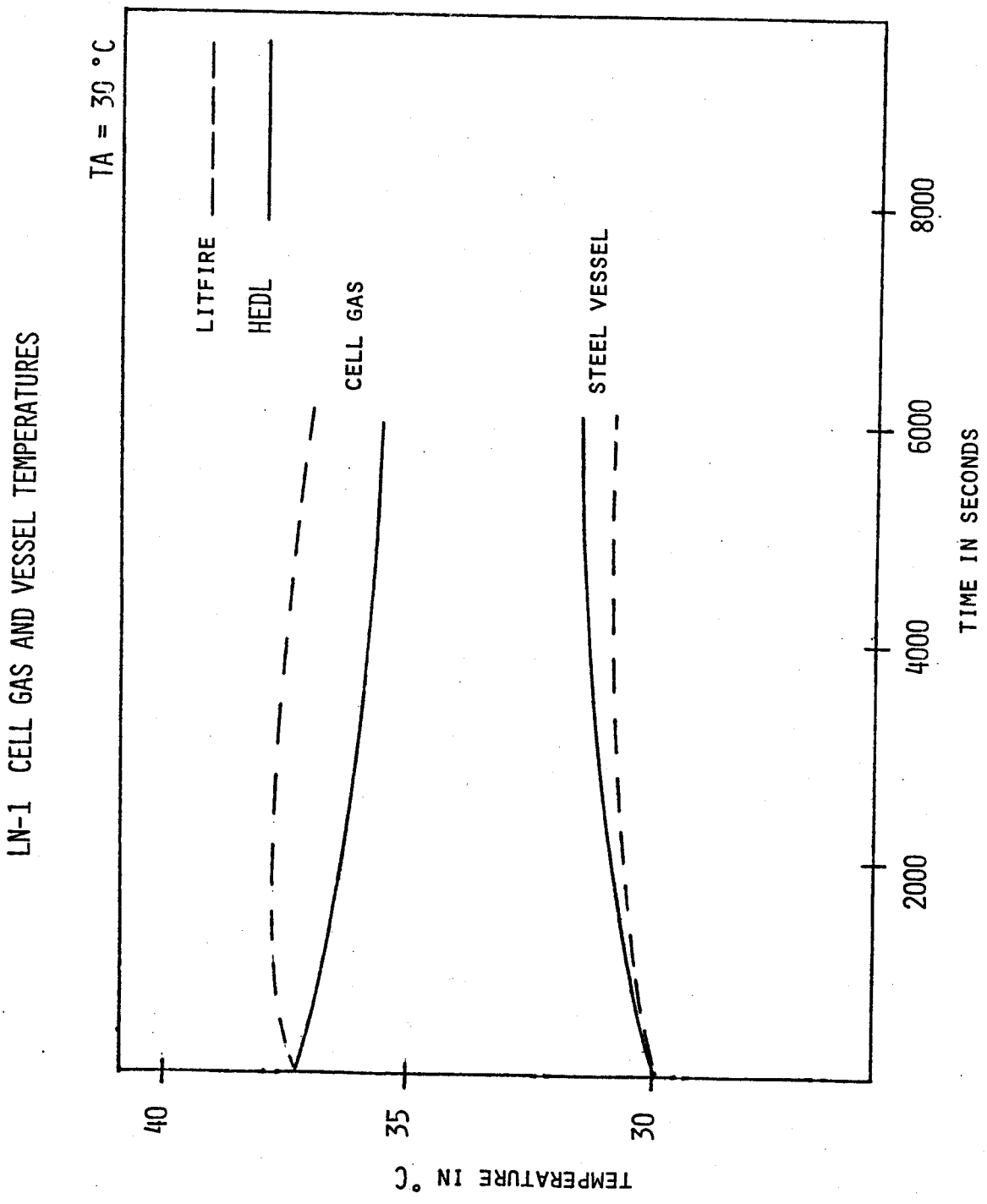
LN-1 CELL GAS AND VESSEL TEMPERATURES
TA = 30 °C
LITFIRE
HEDL
CELL GAS
STEEL VESSEL
40
35
30
TEMPERATURE IN °C
2000
4000
6000
8000
TIME IN SECONDS

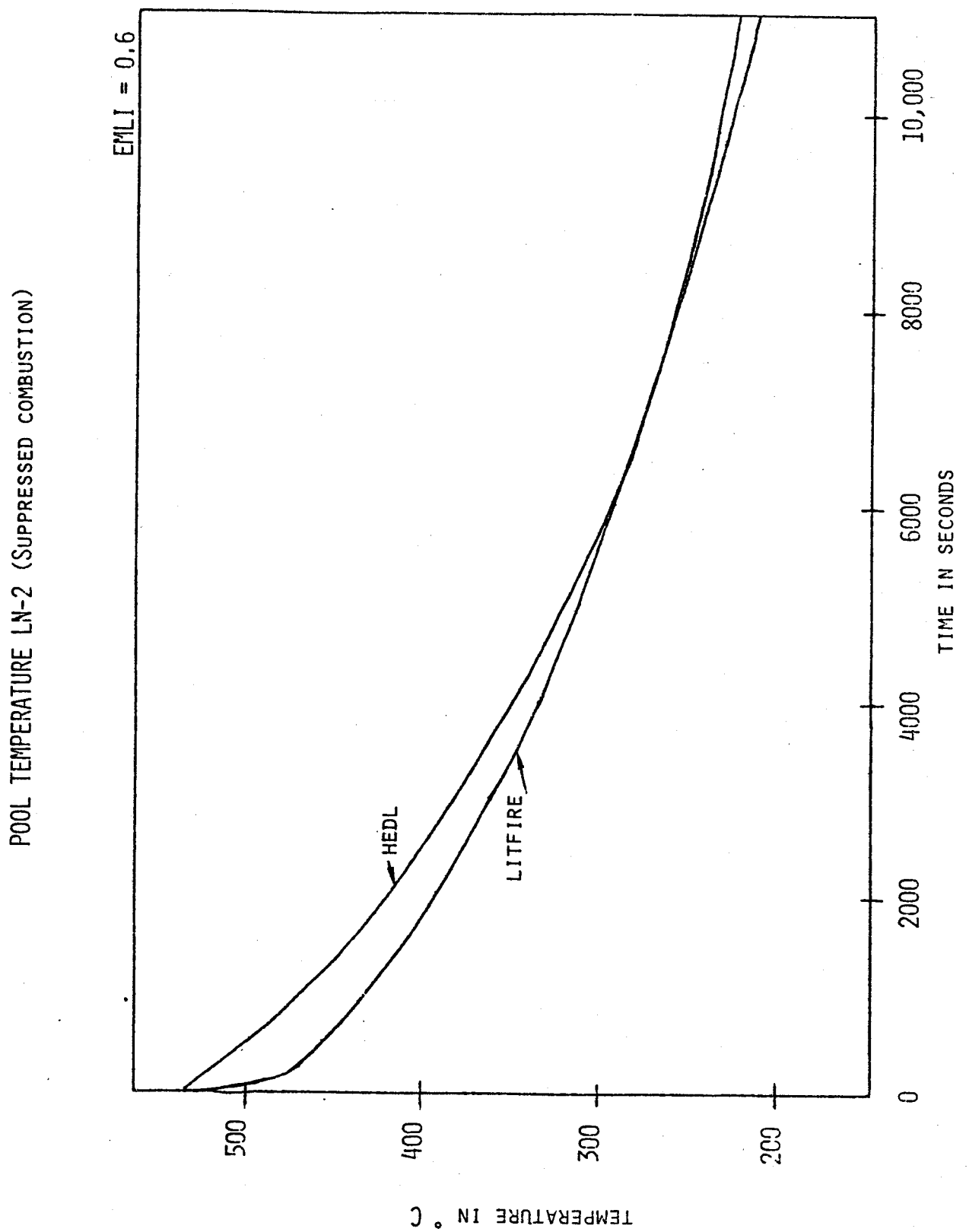
POOL TEMPERATURE LN-2 (SUPPRESSED COMBUSTION)
EMLI = 0.6
HEDL
LITFIRE
TEMPERATURE IN °C
500
400
300
200
0
2000
4000
6000
8000
10,000
TIME IN SECONDS

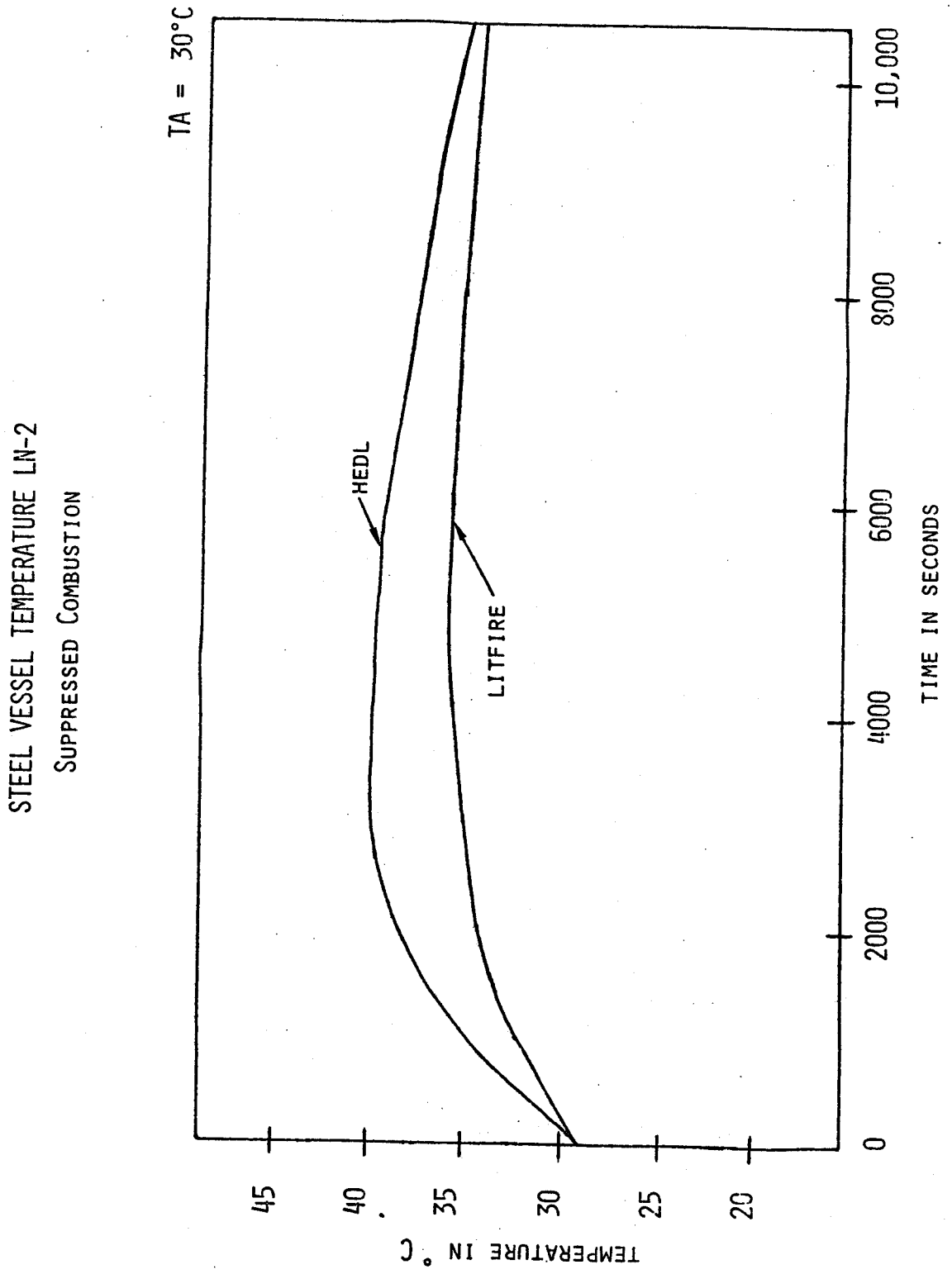
STEEL VESSEL TEMPERATURE LN-2
SUPPRESSED COMBUSTION
TA = 30°C
HEDL
LITFIRE
TEMPERATURE IN °C
45
40
35
30
25
20
0
2000
4000
6000
8000
10,000
TIME IN SECONDS

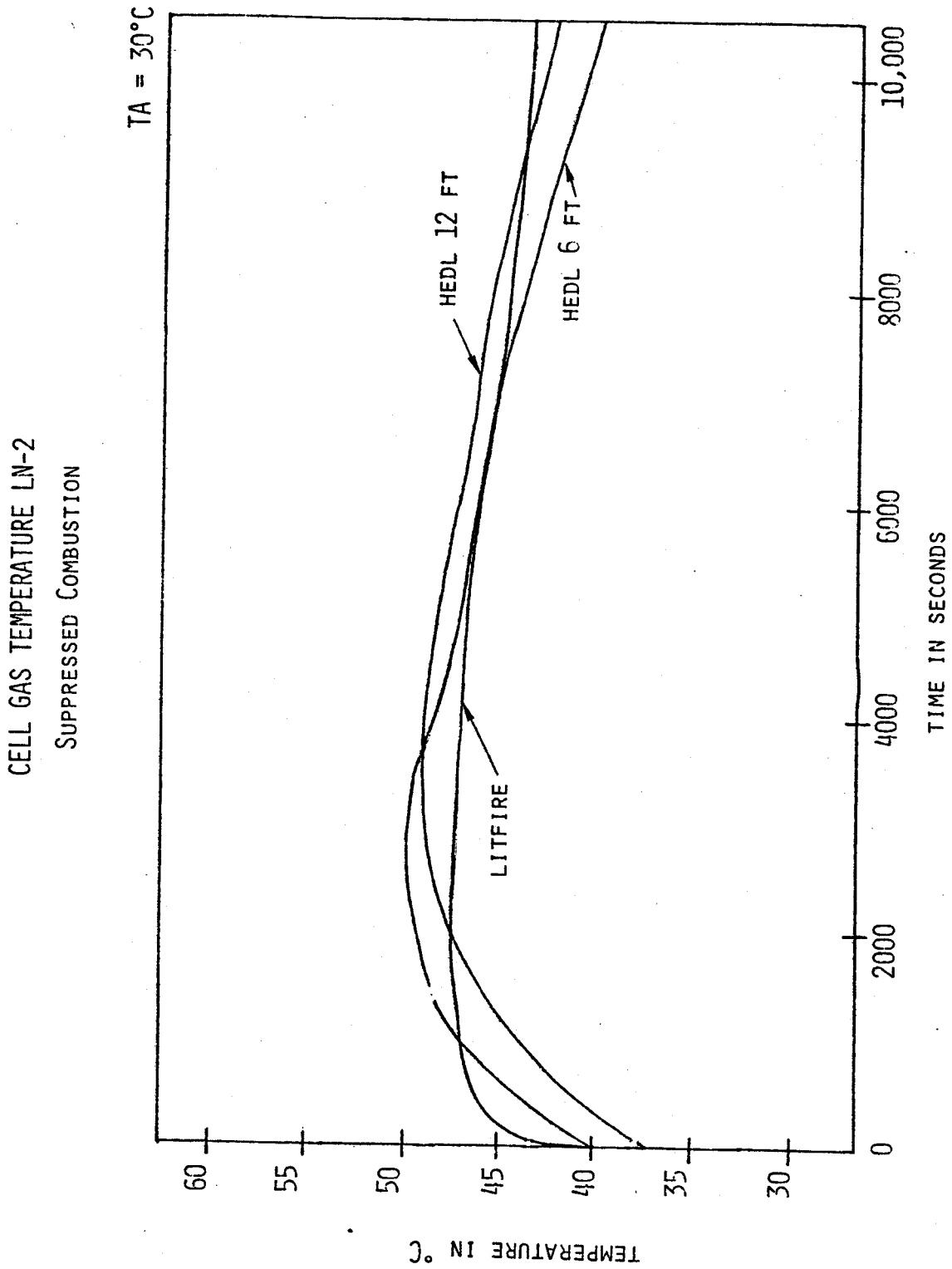
CELL GAS TEMPERATURE LN-2
SUPPRESSED COMBUSTION
TA = 30°C
HEDL 12 FT
HEDL 6 FT
LITFIRE
TEMPERATURE IN °C
TIME IN SECONDS
60
55
50
45
40
35
30
0
2000
4000
6000
8000
10,000

LN-3 REACTION PAN TEMPERATURE (BOTTOM)

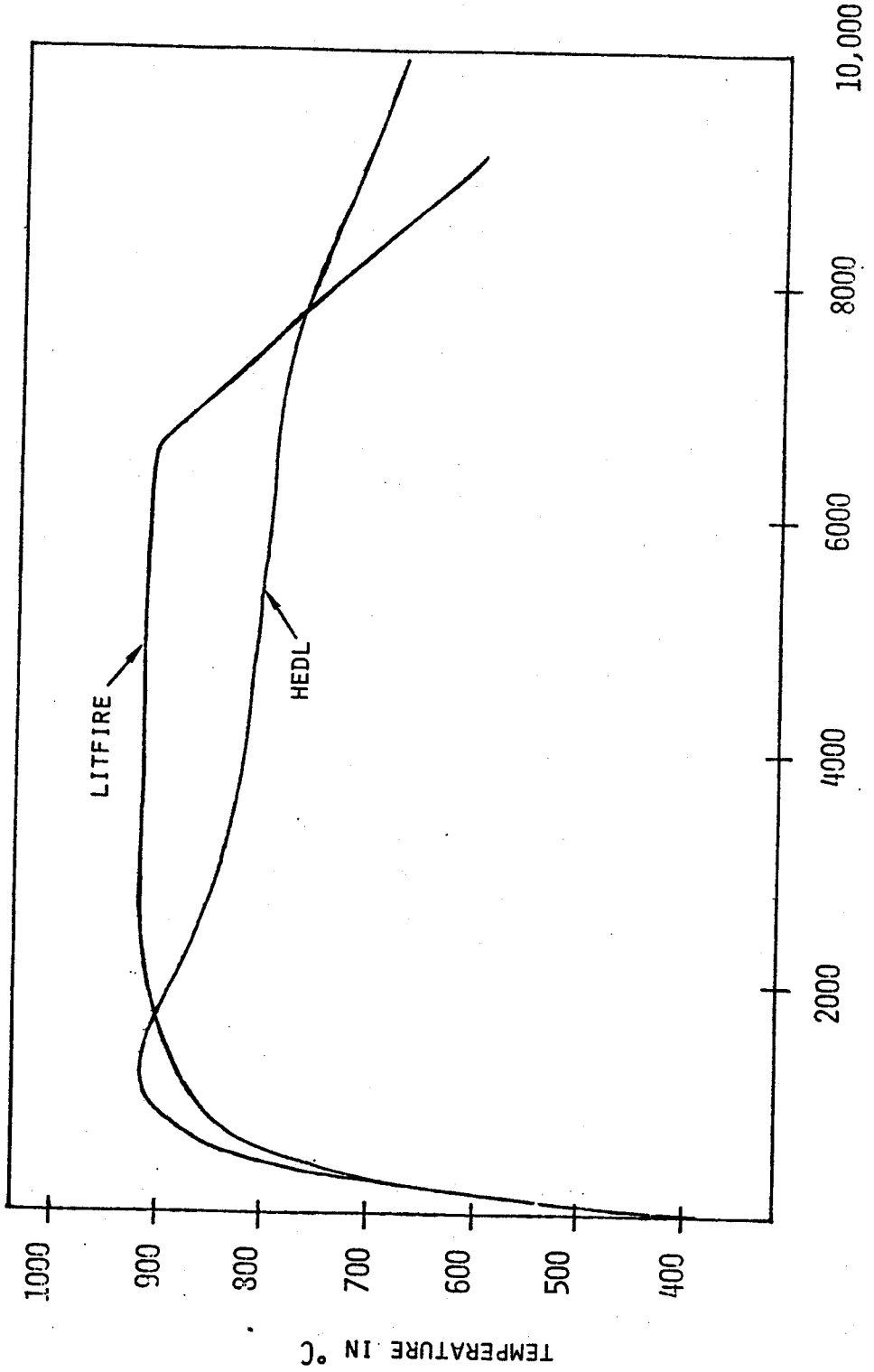

STEEL VESSEL TEMPERATURE LN-3

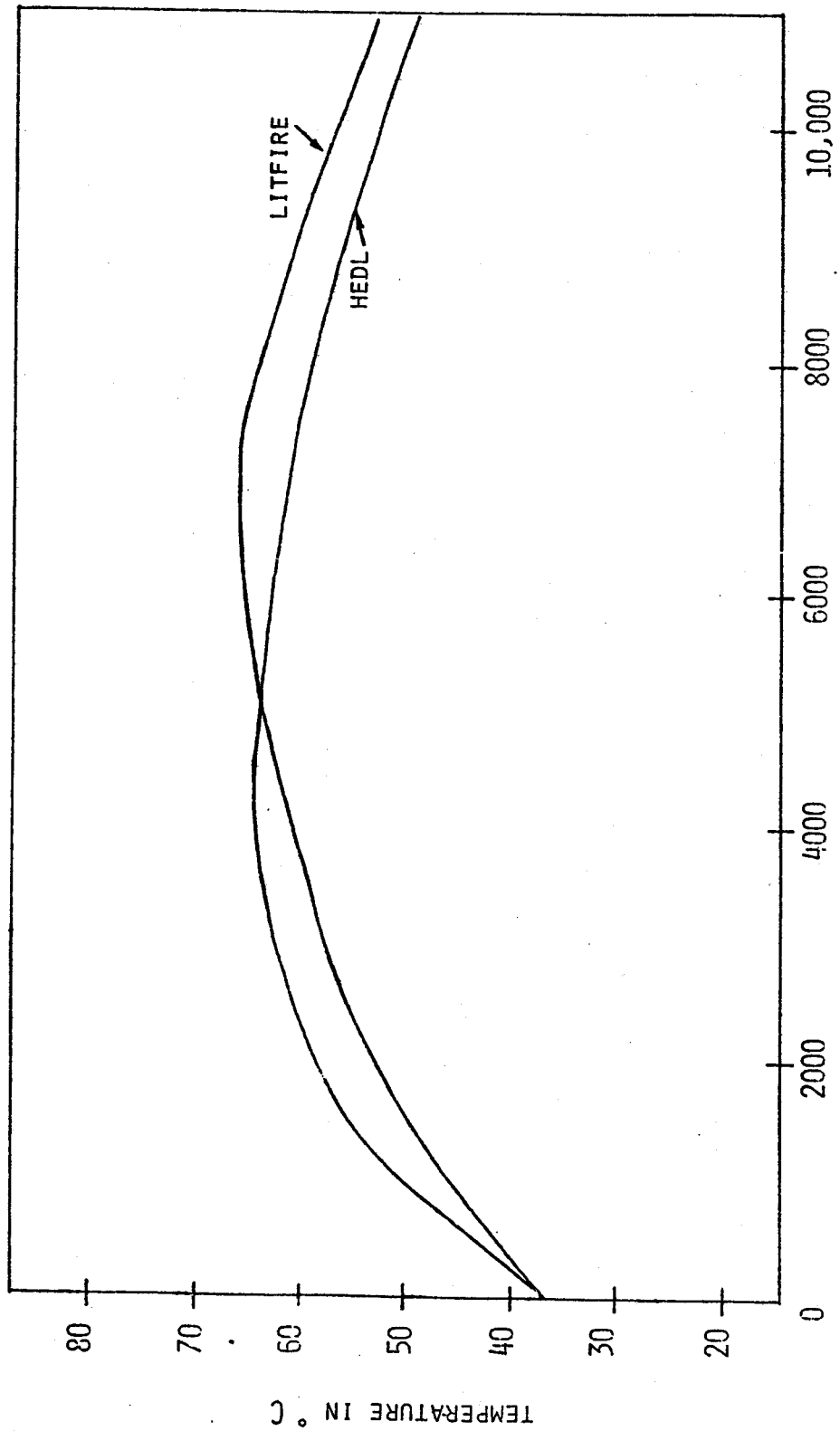

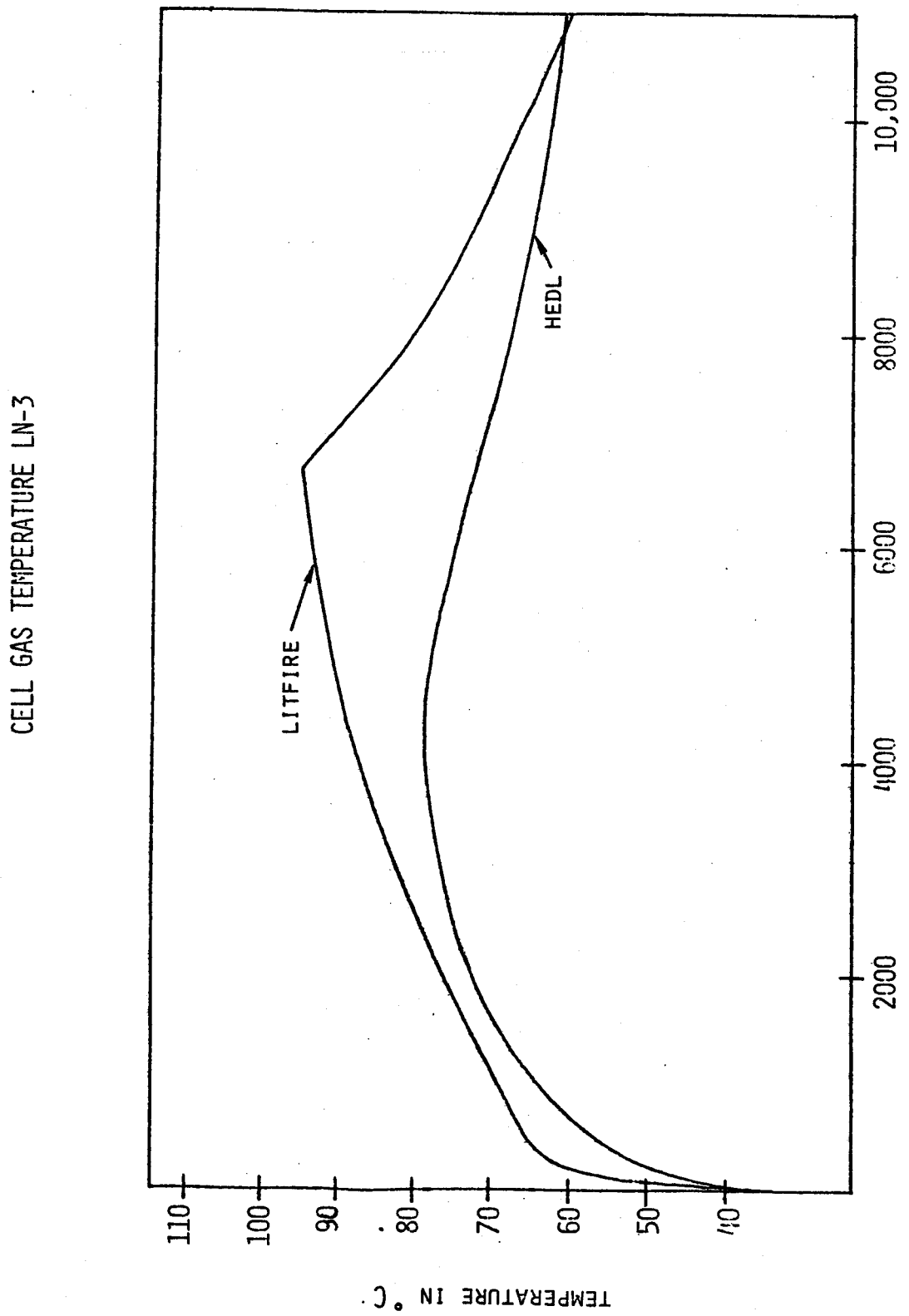
CELL GAS TEMPERATURE LN-3
TEMPERATURE IN °C.
110
100
90
80
70
60
50
40
2000
4000
6000
8000
10,000
TIME IN SECONDS
LITFIRE
HEDL

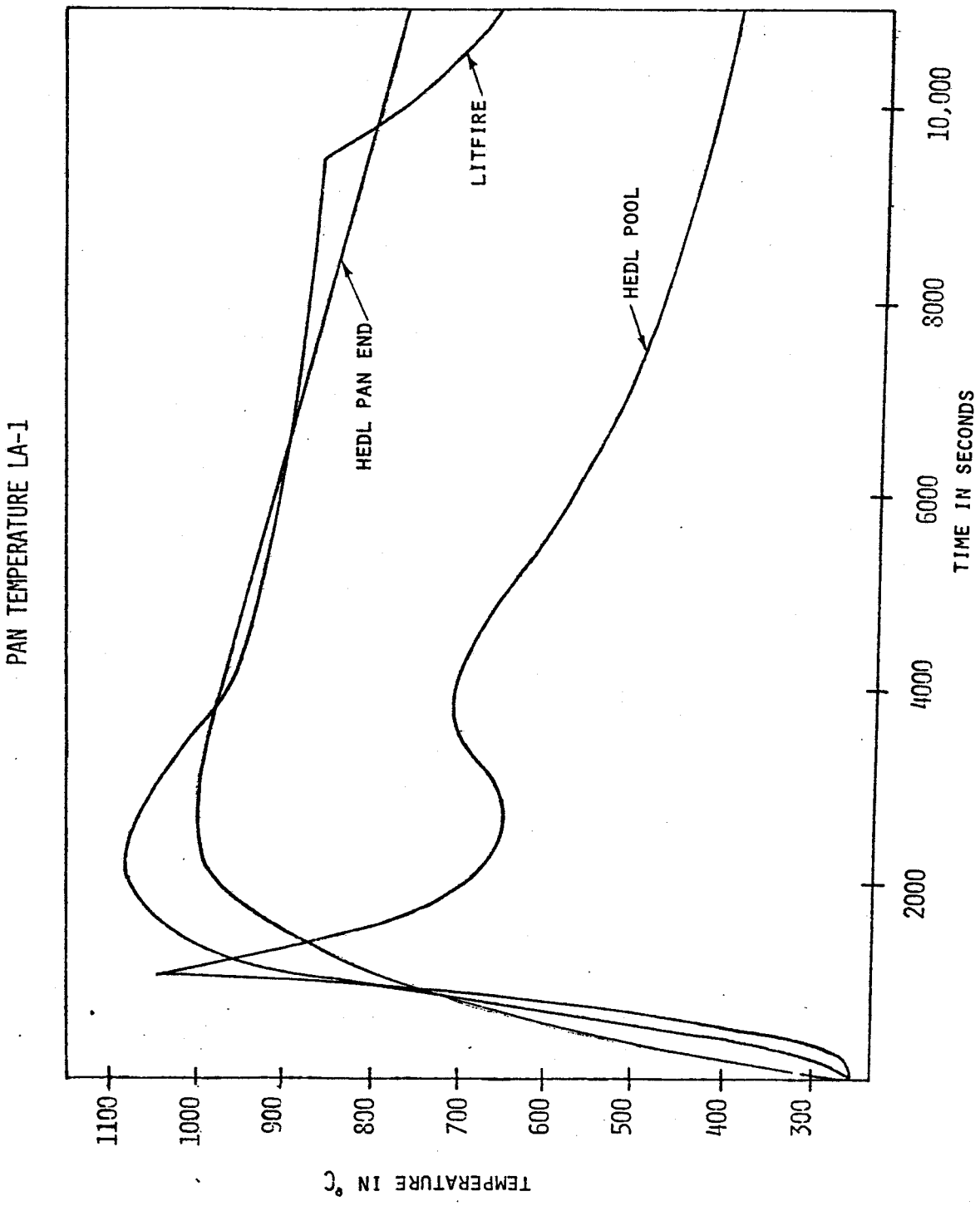
PAN TEMPERATURE LA-1
TEMPERATURE IN °C
1100
1000
900
800
700
600
500
400
300
2000
4000
6000
8000
10,000
TIME IN SECONDS
HEDL PAN END
LITFIRE
HEDL POOL

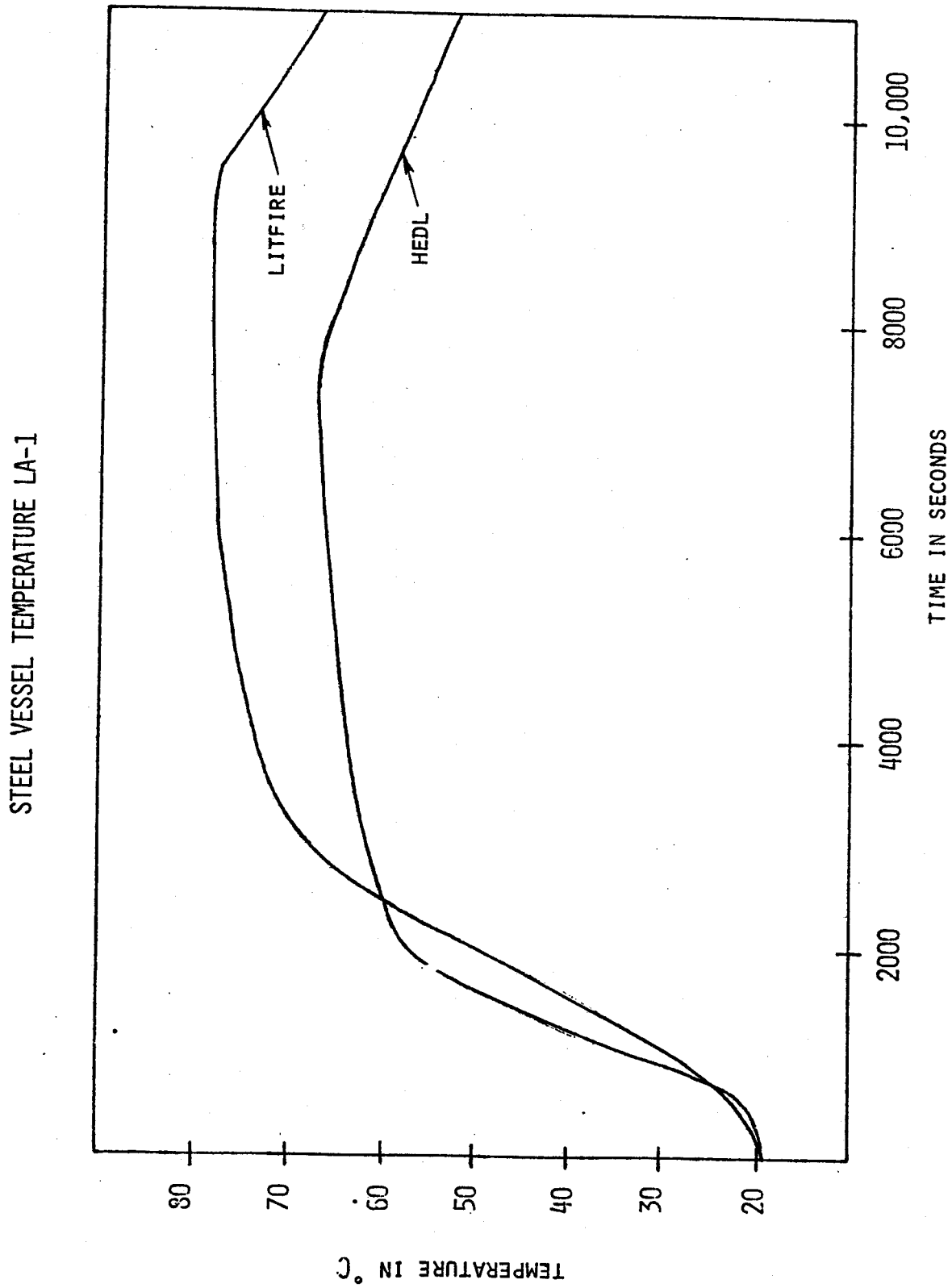
STEEL VESSEL TEMPERATURE LA-1
LITFIRE
HEDL
TEMPERATURE IN °C
80
70
60
50
40
30
20
2000
4000
6000
8000
10,000
TIME IN SECONDS

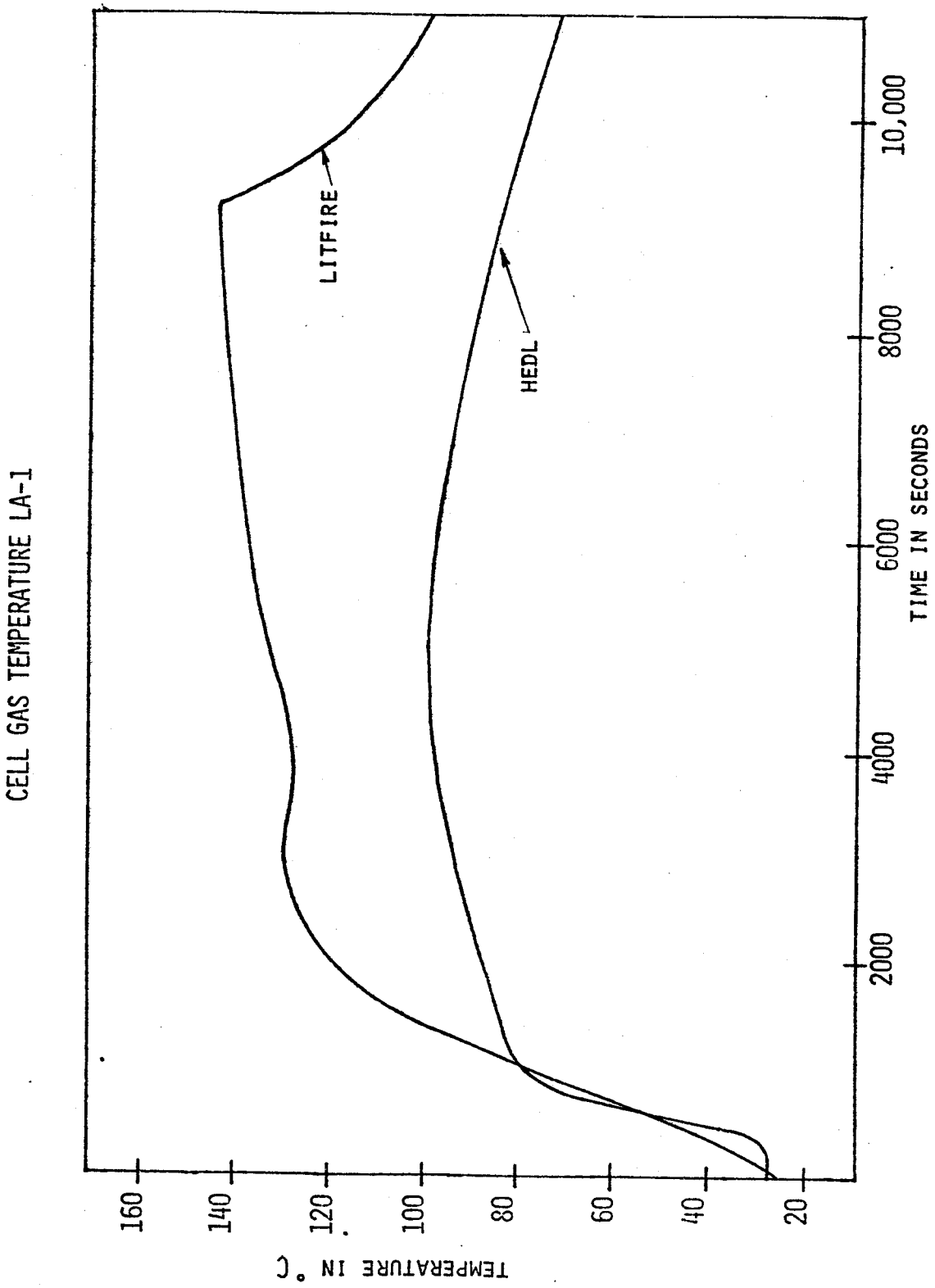
CELL GAS TEMPERATURE LA-1
LITFIRE
HEDL
TEMPERATURE IN °C
160
140
120
100
80
60
40
20
2000
4000
6000
8000
10,000
TIME IN SECONDS

PAN TEMPERATURE LA-2

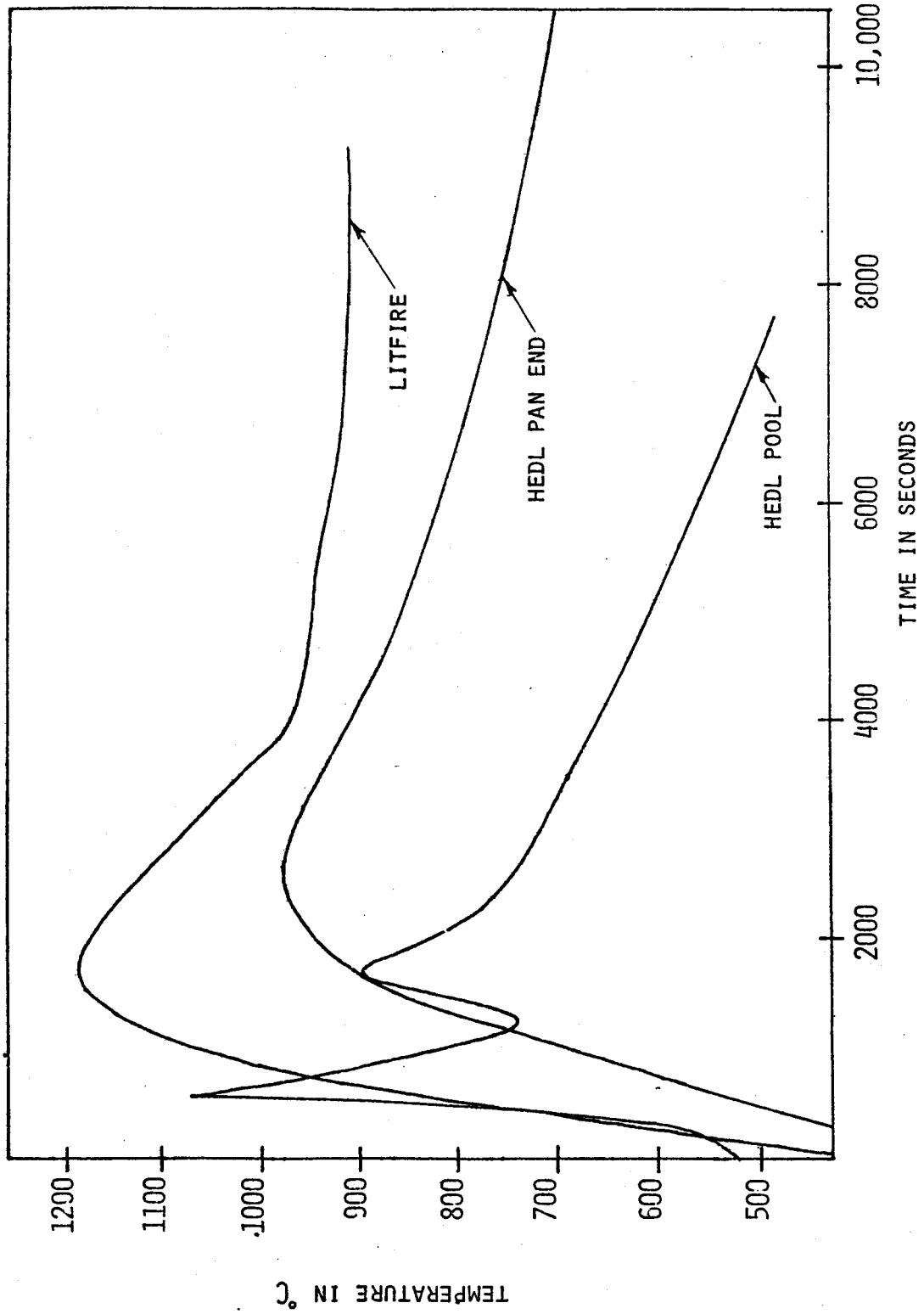

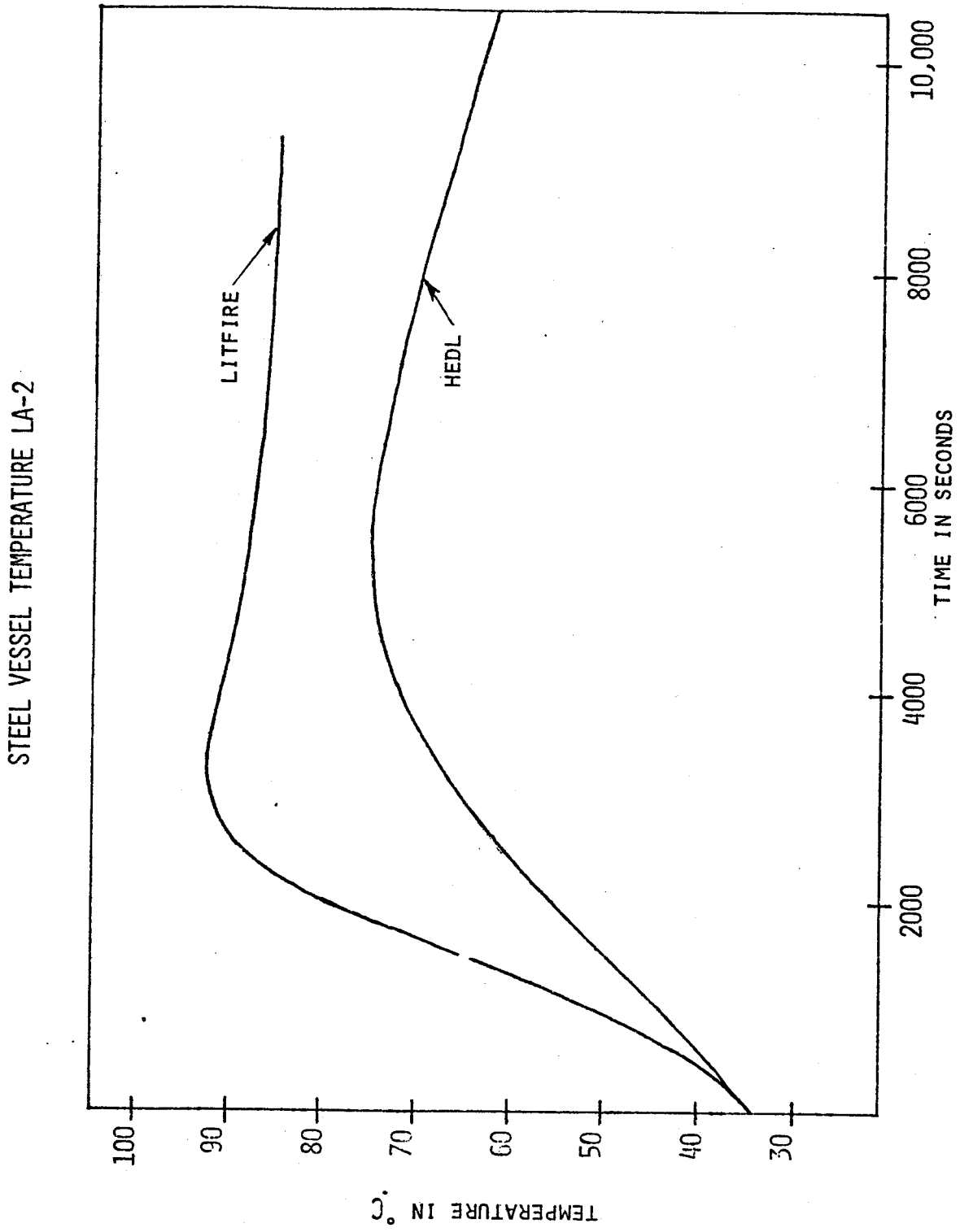
STEEL VESSEL TEMPERATURE LA-2
LITFIRE
HEDL
100
90
80
70
60
50
40
30
TEMPERATURE IN °C
2000
4000
6000
8000
10,000
TIME IN SECONDS

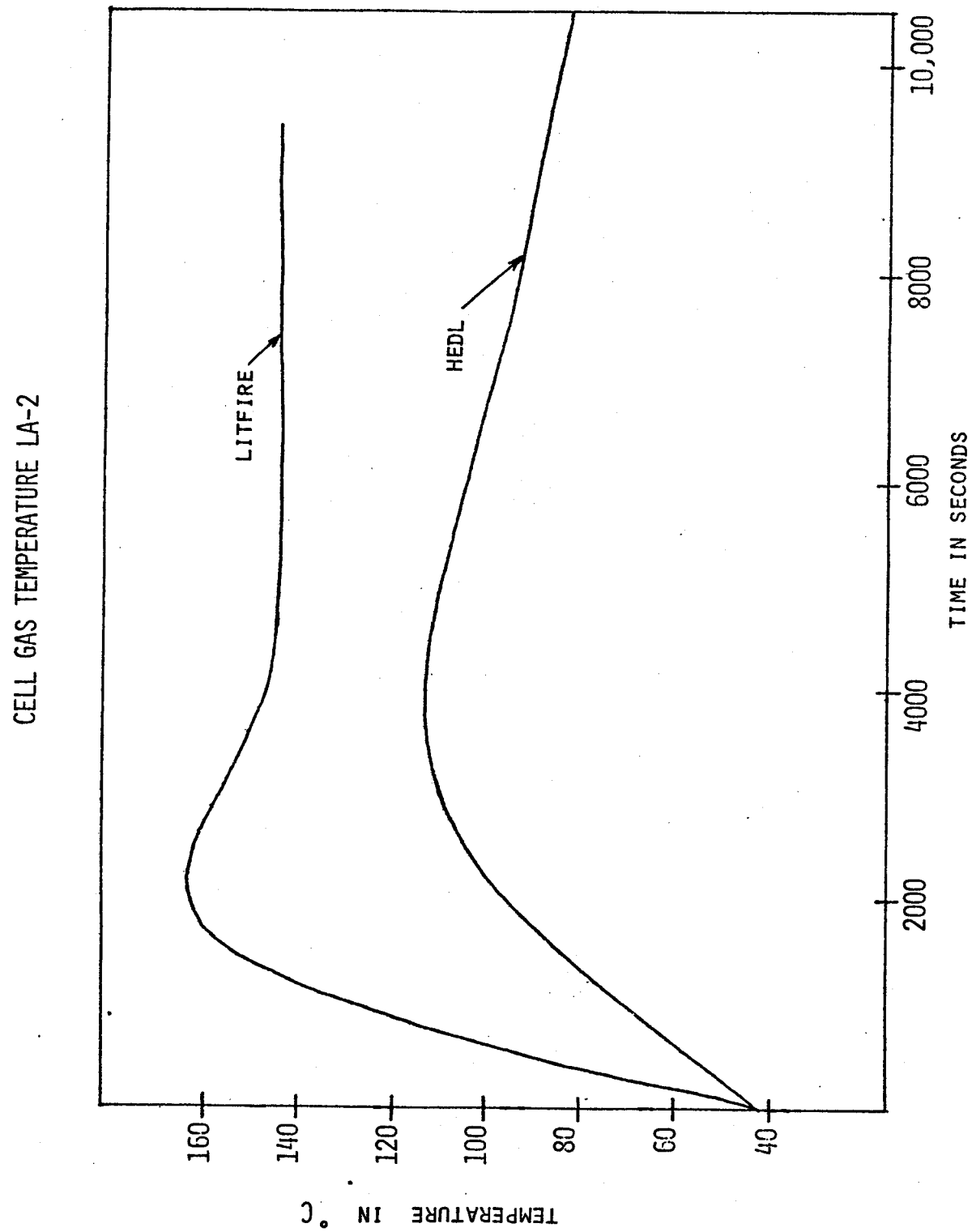
CELL GAS TEMPERATURE LA-2
LITFIRE
HEDL
160
140
120
100
80
60
40
TEMPERATURE IN °C
2000
4000
6000
8000
10,000
TIME IN SECONDS